nature communications

Article

https://doi.org/10.1038/s41467-026-68885-4

Inhibition of TGF-β signaling in microglia stimulates hippocampal adult neurogenesis and reduces anxiety-like behavior in adult mice

Received: 23 April 2025

Accepted: 5 January 2026

Published online: 09 February 2026

Check for updates

Kierra Ware[1], Joshua Peter[1], Jake Yazell[2], Christina Thapa[3], Aleksandr Taranov[2], Alicia Bedolla[2], Claire Distel[1], Sven Lammich[4], Regina Feederle[5,6,7], Alice Sülzen[5], Shane Liddelow[8,9,10], Krishna Roskin[11,12] & Yu Luo[1,2,13]

Adult neurogenesis in the subgranular zone (SGZ) has been implicated in cognitive and affective functions. The role of neuroinflammation and reactive microglia in SGZ neurogenesis is not well understood. TGF-β signaling is critical to maintaining microglia homeostasis in the adult brain. To investigate the role of microglia in SGZ neurogenesis, using microglia-specific inducible knockout (iKO) mice for TGF-β1 ligand or receptor (*Alk5* or *Tgfbr2*), here we show that TGF-β-deficient microglia increase adult neurogenesis in the SGZ, accompanied by altered anxiety-like behavior in KO mice. Single-cell RNAseq (ScRNAseq) analysis shows decreased PTEN signaling, and immunohistochemistry shows increased mTOR activity in DCX+ newly born neuroblasts at the SGZ in iKO mice. Inhibition of mTOR signaling by rapamycin reverses the heightened SGZ neurogenesis in iKO mice. This study reveals the role of microglia in regulating hippocampal adult neurogenesis via the PTEN-mTOR pathway and its potential implications for behavioral and affective functions.

The process by which new neurons are generated in the adult brain is known as adult neurogenesis[1], which predominantly takes place in two neurogenic regions: the subventricular zone (SVZ) and the subgranular zone (SGZ) in the adult mouse brain. The SVZ adult neurogenesis is crucial for processing olfactory sensory information[2,3] and neurorepair after injury[4–6], while the SGZ plays an essential role in pattern separation, forgetting, and affective function regulation[7–11]. Adult neurogenesis is a highly dynamic process that can be regulated by exercise[12], an enriched environment[13,14], and pathological conditions such as stroke[4,6] and epilepsy[15]. However, enhanced neurogenesis has been shown to be both beneficial[5,16,17] or detrimental under pathological conditions[15]. Similarly, the role of microglia and

[1]Department of Molecular and Cellular Biosciences, University of Cincinnati, Cincinnati, OH, USA. [2]Neuroscience Graduate Program, University of Cincinnati, Cincinnati, OH, USA. [3]Center for Psychiatric Genetics, NorthShore University HealthSystem, Evanston, IL, USA. [4]Biomedical Center Munich (BMC), LMU Munich, 81377 Munich, Germany. [5]German Center for Neurodegenerative Diseases (DZNE), 81377 Munich, Germany. [6]Core Facility Monoclonal Antibodies, Helmholtz Munich, German Research Center for Environmental Health, 85764 Neuherberg, Germany. [7]Munich Cluster for Systems Neurology (SyNergy), 81377 Munich, Germany. [8]Institute for Translational Neuroscience, NYU Grossman School of Medicine, New York, NY, USA. [9]Departments of Neuroscience and of Ophthalmology, NYU Grossman School of Medicine, New York, NY, USA. [10]Parekh Center for Interdisciplinary Neurology, NYU Grossman School of Medicine, New York, NY, USA. [11]Department of Pediatrics, University of Cincinnati College of Medicine, Cincinnati, OH, USA. [12]Division of Biomedical Informatics, Cincinnati Children's Hospital Medical Center, Cincinnati, USA. [13]Immunology Graduate Program, Cincinnati Children's Hospital Medical Center and the University of Cincinnati College of Medicine, Cincinnati, OH, USA. e-mail: luoy2@ucmail.uc.edu

neuroinflammation in adult neurogenesis has been under debate. Specifically, it has been speculated that neuroinflammation resulting from CNS injury or disease might be detrimental to adult neurogenesis[6,18–21]. However, CNS injuries (stroke or traumatic brain injury (TBI)) or pathological conditions (epilepsy), which are accompanied by neuroinflammation and reactive microglia, can transiently stimulate neurogenesis[15,22,23]. Additionally, while the role of microglia in subventricular zone (SVZ) neurogenesis has recently been explored during brain development and adulthood[24–27], its role in SGZ neurogenesis under physiological and pathological conditions is less understood[28,29]. Understanding the role and mechanisms of microglia in regulating adult SGZ neurogenesis and dentate gyrus (DG) sprouting might provide additional therapeutic targets to enhance beneficial or inhibit detrimental neurogenesis.

Microglia are the innate immune cells in the brain and act as a first line of defense when the brain is under duress[30]. The transition from a homeostatic state to a reactive phenotype in microglia is a key hallmark of their sensitivity to the surrounding microenvironment[31–34]. Their unparalleled capacity to sense and respond to changes in the brain's microenvironment via pattern recognition receptors (PRRs), and specialized receptors such as purinergic receptors (P2RY) or Triggering Receptor Expressed On Myeloid Cells 2 (TREM2) make microglia master regulators of various processes, ranging from immune responses to synaptic pruning. Recently, microglia have been implicated in playing a critical role in regulating adult SVZ neurogenesis in mice[24–27]. Specifically, microglia ablation studies have been used to assess their functions in adult neurogenesis in the SVZ. Microglia ablation globally[26] or in the SVZ locally[24] did not reduce the proliferation and early differentiation of SVZ neural stem cells (NSCs). Rather, microglia might be critical for the migration of newly born neuroblasts and the pruning of dendritic spines of newly born neurons, as microglia-ablated mice show reduced migration of newly born neurons to the olfactory bulb[24] (OB) and reduced synaptic dendritic spines in the newly born neurons in OB[25]. Overall, the precise roles and mechanisms of microglia in regulating SGZ adult neurogenesis under both homeostatic and reactive states remain largely unknown. However, there is key evidence that supports a direct regulatory role of microglia in adult hippocampal neurogenesis. For example, one study reported that microglia phagocytose apoptotic neuroblasts in the SGZ[29], which was later shown to be critical in maintaining adult SGZ neurogenesis[28]. Additionally, under pathological conditions, microglia ablation abolished epilepsy-induced SGZ neurogenesis[35], suggesting that in epilepsy, reactive microglia might contribute to the increased SGZ neurogenesis, possibly through the function of P2RY12[35]. In summary, these findings underscore a potentially critical role of microglia in regulating adult neurogenesis under physiological and pathological conditions. However, due to the complex cellular environment in vivo, especially after injury, the precise contribution of microglia to neurogenesis and the signaling pathways that mediate these interactions remain challenging to decipher. One common factor in conditions where microglia might be critical for neurogenesis is a reactive microglial profile (e.g., after injury, stroke, or pathological conditions in epilepsy) or a developmentally regulated microglial profile during embryonic development. This prompts the question of whether a reactive or developmentally regulated microglia profile could causally and directly enhance adult neurogenesis. Recent studies by us[36] and others[37,38] showed that altering microglia-derived TGF-β signaling, either through ligand or receptor knockout (KO) in microglia, leads to loss of microglia homeostasis. This shift of microglial homeostatic status results in transcriptomic profiles resembling those of aged, disease-related, and injury-related microglia[36]. Using these microglia-specific mouse models targeting TGF-β signaling, we aim to determine whether manipulating the TGF-β signaling pathway in microglia can directly affect adult neurogenesis in the SGZ. Our results show that, indeed, abolishing TGF-β signaling in microglia via the loss of the TGF-β1 ligand or via loss of function of the ALK5 (type 1) or TβRII (type 2) receptors all lead to an altered microglia profile that is sufficient to transiently stimulate SGZ adult neurogenesis. This finding establishes a direct role of microglial profile in regulating SGZ neurogenesis, independent of disease models like stroke, TBI, or epilepsy, providing a clean model to study microglia-NSC crosstalk. In our study, using this as a microglia-NSC crosstalk model, we also investigate the functional outcome of this heightened SGZ neurogenesis in anxiety-related behavior tests (elevated plus or elevated zero maze), which have been linked to SGZ adult neurogenesis[8,10]. Additionally, using scRNAseq analysis and functional validation by double KO mouse models and pharmacological inhibition, we investigate several candidate molecular pathways that could potentially mediate this cell-cell crosstalk, identified by scRNAseq and cell-cell interaction analysis. In summary, in contrast to the prevailing hypothesis that inflammatory microglia are, in general, detrimental to SGZ adult neurogenesis, our results show that microglia made reactive by silencing of TGF-β signaling can stimulate adult SGZ neurogenesis. Our data also show that microglia-derived Insulin-like Growth Factor 1 (IGF-1) or Tumor Necrosis Factor-Alpha (TNF-α) are not required for this stimulatory effect; instead, it is mediated by the upregulation of epilepsy-related genes and alterations in the PTEN-mTOR pathways in the iKO mice.

Results

The absence of *Alk5*-mediated TGF-β signaling in microglia results in the downregulation of microglia homeostatic genes and microgliosis, but not astrogliosis, in the adult mouse brain

We previously showed that the deletion of microglia-derived *Tgfb1* ligand results in the loss of microglial homeostatic morphology and transcriptomic profile[36]. We also showed that this loss of homeostasis in microglia is due to direct loss of TGF-β signaling in microglia and not that of astrocytes, as deletion of the type 1 TGF-β receptor *Alk5* in microglia leads to a similar phenotype in microglia, while *Alk5* deletion in astrocytes does not[36]. To investigate how the loss of TGF-β signaling in microglia and its subsequent induction of reactive profiles might affect adult neurogenesis, we first utilize the microglia-specific receptor knockout mice in this study to avoid potential caveats of the direct effect of loss of microglia-derived TGF-β ligand on adult neurogenesis. Microglia-specific *Alk5* inducible knockout mice were generated by crossing the $Cx3cr1^{CreER}$ line with the $Alk5^{fl/fl}$ line to ablate *Alk5*-mediated signaling in myeloid cells (Microglia, boarder-associated macrophage-BAMs, and peripheral monocytes/macrophages) during adulthood upon tamoxifen (TAM) administration (Fig. 1A). A R26-YFP (yellow fluorescent protein) reporter allele is also bred in both $Cx3cr1^{CreER}$-$Alk5^{WT/WT}$ and $Cx3cr1^{CreER}$-$Alk5^{fl/fl}$ mice to label recombined microglia and facilitate microglia sorting. Young adult $Cx3cr1^{CreER}$-$Alk5^{WT/WT}$ or $Cx3cr1^{CreER}$-$Alk5^{fl/fl}$ mice were harvested 3 weeks post TAM treatment (Fig. 1A), a timepoint allowing the majority of peripheral monocytes/macrophages to replenish from CX3CR1-negative progenitors, to minimize the effect of gene knockout on monocytes. Our previous study shows that this TAM regimen in the $Cx3cr1^{CreER}$-$Alk5^{fl/fl}$ iKO mice efficiently deletes floxed *Alk5* alleles in brain macrophages[36] but shows no differences in *Alk5* mRNA levels in blood or splenic monocytes (Supplementary Fig. 1). Compared to $Cx3cr1^{CreER}$-$Alk5^{WT/WT}$ control mice (Fig. 1B), microglia displayed a reduction in homeostatic markers such as *P2ry12* and *Tmem119* in $Cx3cr1^{CreER}$-$Alk5^{fl/fl}$ mice (Fig. 1C). Consistently, from sorted brain microglia and BAMs (YFP +), we demonstrate a significant decrease in *Alk5, Tmem119*, and *P2ry12* mRNA levels (Fig. 1D) in $Cx3cr1^{CreER}$-$Alk5^{fl/fl}$ mice in comparison to control microglia from $Cx3cr1^{CreER}$-$Alk5^{WT/WT}$ (Fig. 1E–G) mice. Moreover, the pro-inflammatory cytokine *Tnf* was upregulated in microglia sorted from $Cx3cr1^{CreER}$-$Alk5^{fl/fl}$ *mice* (Fig. 1H). *Tnf* expression levels are not altered in the blood or splenic monocytes (Supplementary Fig. 1), supporting the CNS-specific modulation of this pathway in our mouse model. Taken together, the downregulation of homeostatic markers

https://doi.org/10.1038/s41467-026-68885-4

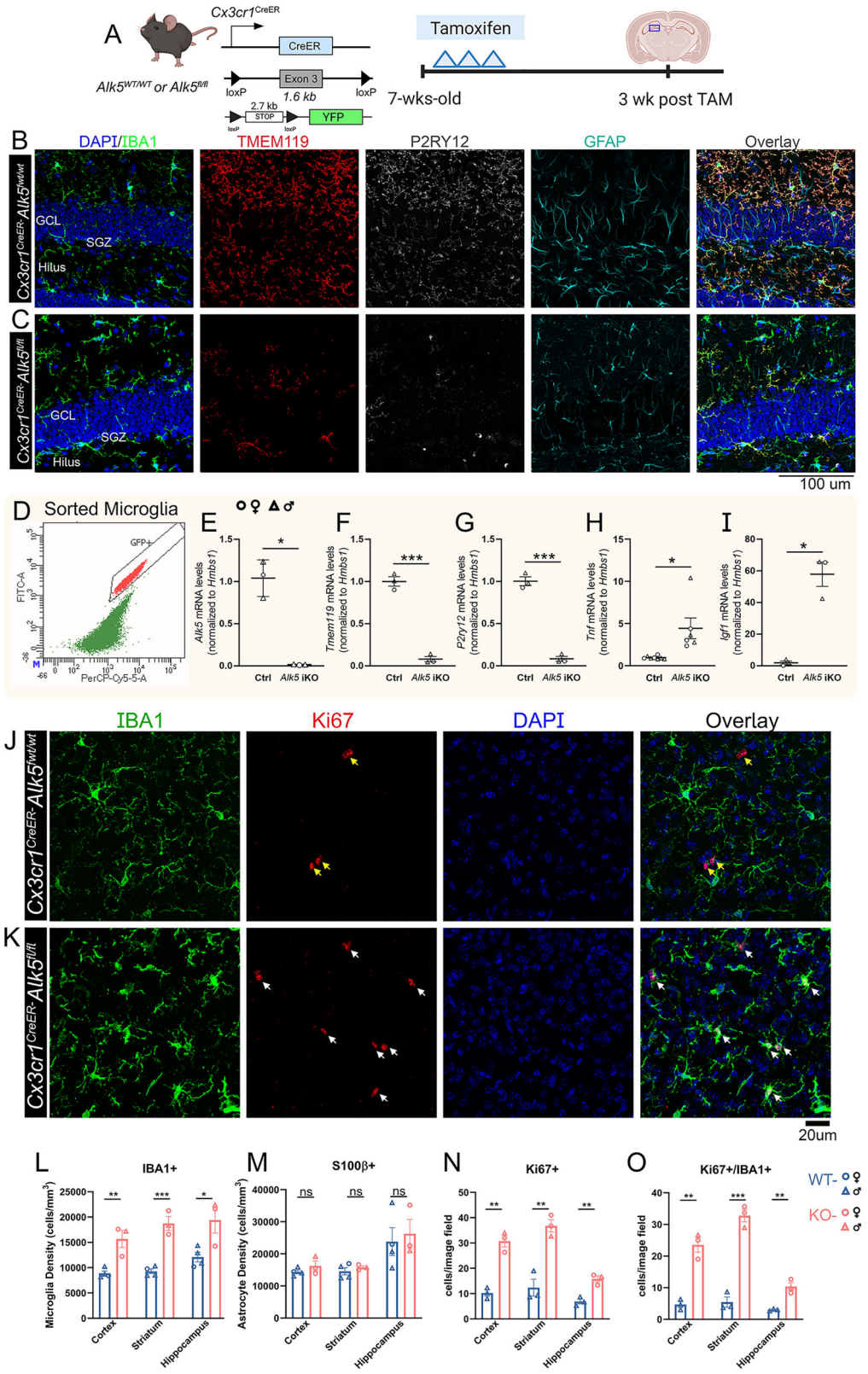

and the upregulation of pro-inflammatory cytokines indicate a reactive phenotype of microglia. Additionally, *Igf1*, an essential growth factor to embryonic and adult neurogenesis, was also significantly upregulated in *Cx3cr1*^{CreER}-*Alk5*$^{fl/fl}$ (Fig. 1I), consistent with our previous results from the MG-*Tgfb1* iKO microglia, suggesting a potential effect in the regulation of adult neurogenesis of these young adult mice, given previous stipulations on IGF-1's role in neurogenesis[39–41]. Consistent with our report in MG-*Tgfb1* iKO mice, total microglia (IBA1+) cells in cortex, striatum, and hippocampus increase in MG-*Alk5* iKO mice compared to control mice (Fig. 1L, N, O) while total astrocytes (S100β+) number remains the same in MG-*Alk5* iKO mice (Fig. 1M). Corroborating an increased number of IBA1+ microglia in the iKO mice, there was a significant increase in the number of Ki67+ cells (Fig. 1K, N). Additionally, the majority of Ki67+ cells colocalized with IBA1+ cells

Fig. 1 | Deletion of *Alk5* gene in adult microglia results in microglial dyshomeostasis and microgliosis but not astrogliosis in the adult mouse brain. A A mouse model and experimental timeline for targeting microglial *Alk5* and analyzing microglia homeostatic marker expression and microgliosis 3 weeks post tamoxifen. **B**, **C** Representative images of the hippocampus stained for IBA1, TMEM119, P2RY12 (BioLegend Ab), and GFAP in **B** *Cx3cr1*^{CreER}-*ALK5*$^{wt/wt}$ or **C** *Cx3cr1*^{CreER}-*ALK5*$^{fl/fl}$ mice **D** FACS-sorted GFP+ microglia were analyzed for mRNA levels using qRT-PCR showing **E** *Alk5* (indicating gene deletion efficiency), **F** Tmem119, **G** P2ry12, **H** Tnf, and **I** *Igf1* expression levels in control and iKO microglia (**E**–**I**) ($n = 3$ for control, $n = 3$ for *Alk5* KO, * $p = 0.0146$ for panel E, *** $p = 0.0005$ for panel F, *** $p = 0.0004$ for panel G, * $p = 0.0372$ for panel H, * $p = 0.0167$ for panel I, two-sided student's t-test was used for statistical analysis for panels E-I). Representative immunohistochemistry images of IBA1, Ki67, and DAPI in the cortex of **J** *Cx3cr1*^{CreER}-*ALK5*$^{wt/wt}$ or **K** *Cx3cr1*^{CreER}-*ALK5*$^{fl/fl}$ at 3 weeks after TAM treatment. Arrows show Ki67+ cells (yellow arrows show Ki67+ cells not co-localized with IBA1+ cells and white arrows show Ki67+ cells co-localizing with IBA1+ cells). Unbiased stereological quantification for **L** Microglia density, **M** Astrocyte density, **N** total number of Ki67+ cells, and **O** the number of IBA1 + /Ki67+ cells (**L**–**O**) ($n = 4$ for control, $n = 3$ for *Alk5* KO, ** $p = 0.002$, *** $p < 0.001$, and ** $p = 0.001$ for panel L, ns = not significant for panel **M**, ** $p < 0.001$, $p < 0.00$, and $p = 0.011$ for panel **N**, ** $p < 0.001$, *** $p < 0.001$, and ** $p = 0.006$ for panel **O**, two-sided 2-way ANOVA with Tukey post hoc pairwise comparison was used for statistical analysis for panels **L**–**O**). Each data point represents the average of a single animal (> 3 brain sections per mouse for each brain region). The sex of each animal is represented by open circles (females) and open triangles (males). Mean ± SE. Scale bar as indicated. Panel A was created in BioRender. Luo, A. (2026) https://BioRender.com/0xildk2. Source data are provided as a source data file.

(Fig. 1K, O) in *Cx3cr1*^{CreER}-*ALK5*$^{fl/fl}$ (Fig. 1K), and total IBA1 + /Ki67+ cells also increased in the MG-*Alk5* iKO mice. This is consistent with previous studies suggesting impaired TGF-β signaling in microglia leads to microgliosis[36,42] (Fig. 1L, N, O) but not astrogliosis.

Cx3cr1^{CreER}-*Alk5* iKO mice show a transient increase in hippocampal neurogenesis in young adult mice

CNS injuries (such as stroke or TBI) have been reported to induce microglia reactivity and increase adult neurogenesis in the SGZ[43,44]. To investigate whether there is a direct causal relationship between microglial TGF-β signaling and levels of SGZ adult neurogenesis, we evaluated the impact of *Alk5* deletion in microglia on adult neurogenesis in the hippocampus (SGZ). *Cx3cr1*^{CreER}-*Alk5*$^{WT/WT}$ or *Cx3cr1*^{CreER}-*Alk5*$^{fl/fl}$ mice were harvested at 3-, 6- and 12-weeks post TAM to follow the full maturation cycle of the adult neurogenic cascade (Fig. 2A). BrdU was administered at one-week post TAM injections (Fig. 2A) for 8 days to label dividing cells and subsequently track a cohort of adult-born neurons from proliferation to maturation. MG-*Alk5* iKO mice showed a significant increase (> 66%) in the number of doublecortin (DCX +) cells as compared to control mice (Fig. 2B, E). Consistently, the number of BrdU+ cells increased by greater than 36% in MG-*Alk5* iKO mice at 3 weeks post-TAM (Fig. 2F). Interestingly, by 6- and 12-weeks post-TAM, we no longer observed any significant changes in the amount of DCX+ cells in the SGZ (Fig. 2E), suggesting the increase in a cohort of newly born immature neurons in the SGZ is not sustained. However, BrdU + /NeuN+ cells remained increased at 6 and 12 weeks after TAM (Fig. 2F), supporting that the increased population of immature neuroblasts (DCX +) cells at 3 weeks indeed led to an increased number of adult-born mature neurons at the 6-week and 12-week time points. We also note that there is a significant decrease in total DCX+ cell numbers at 12 weeks post-TAM compared to 3 weeks, consistent with the previously reported age-related decline in SGZ neurogenesis[45,46]. It has been previously reported that only ~30% of newly born cells (identified by BrdU pulse labeling) at SGZ survive to mature neurons[47] and this is recapitulated in our studies as we observe a steady decline of BrdU+ double positive cells over the 3–12-week time course in control mice which show ~30% survival rate in total BrdU+ cells (Fig. 2B–F). In contrast, MG-*Alk5* iKO mice displayed an increased survival rate of ~ 50% in BrdU+ cells during the 3–12-week time frame (Fig. 2F), with both WT and MG-*Alk5* iKO mice showing the expected switch of BrdU + cells from more immature neurons (BrdU + /DCX+ colocalization) at 3 weeks (Fig. 2G) to more mature neurons (BrdU + /NeuN+ colocalization) at 6 and 12 weeks post TAM (Fig. 2H), indicating maturation of neuroblasts to neurons over time. Similarly, the ventral hippocampus exhibits an increase in DCX+ cells and dendritic arborizations at 3 weeks post TAM but recovers to the control level at 6- and 12-weeks post TAM (Supplementary Fig. 2). Furthermore, we observed increased DCX+ dendritic arborization in the hippocampus of the *Cx3cr1*^{CreER}-*Alk5*$^{fl/fl}$ mice (Fig. 2I), consistent with increased DCX+ immature neuron numbers. Taken together, our results show that microglia reactivity caused by loss of microglial TGF-β signaling stimulates adult hippocampal neurogenesis transiently and results in a net gain of a cohort of mature neurons by 6-12 weeks post-TAM. The increase in DCX+ immature neurons observed at 3 weeks in the MG-*Alk5* iKO mice returned to a comparable level to control mice at 6- and 12- weeks post *Alk5* gene deletion in microglia. To examine whether the return of DCX+ cells to the control levels in later time points is due to the recovery of microglia phenotype in the *Cx3cr1*^{CreER}-*Alk5*$^{fl/fl}$ iKO mice, we analyzed the phenotype of microglia from 3 to 12 weeks post TAM treatment and found that, indeed, there is a recovery of morphology, homeostatic marker P2RY12 expression which correlates with recovered nuclear phosphorylated Mothers against decapentaplegic homolog 3 (pSMAD3) levels in IBA1+ cells (Supplementary Fig. 3) at 12 weeks post TAM, supporting that the neurogenesis phenotype is directly linked to the microglia phenotype in the *Cx3cr1*^{CreER}-*Alk5*$^{fl/fl}$ iKO mice.

Loss of microglial type 2 TGF-β receptor or TGF-β1 ligand in microglia recapitulates the phenotype of increased immature neurons at the adult hippocampal niche

Both type 1 and type 2 receptors are required for the formation of the heterotetramer receptor complex that mediates TGF-β signaling[48]. While the type 1 receptor, ALK5, can mediate and is required for TGF-β signaling, it is well documented that other TGF-β superfamily ligands can also signal through this receptor, including ligands from the activin subclass[49]. In contrast, the type 2 receptor, TβRII, exclusively mediates signaling through the TGF-β ligands[50]. Therefore, to further investigate whether the loss of TGF-β signaling or loss of activin signaling via the ALK5 receptor is the cause of the increase in adult neurogenesis we observed in adult mice, we also generated the *Cx3cr1*^{CreER}·*Tgfbr2*$^{fl/fl}$ iKO mouse line (Supplementary Fig. 4A) to not only maximize recombination efficiency but also mitigate the deletion of TGF-β signaling down to just one subclass containing the TGF-β1, 2, and 3 ligands. Following the same experimental timelines, *Cx3cr1*^{CreER}·*Tgfbr2*$^{WT/WT}$ *and Cx3cr1*^{CreER}·*Tgfbr2*$^{fl/fl}$ mice were treated with TAM and harvested at 3 weeks post-TAM (Supplementary Fig. 4A). Our results are consistent with the MG-*Alk5* iKO mice (Figs. 1, 2) in that homeostatic markers *Tmem119* and *P2ry12* for microglia are downregulated (Supplementary Fig. 4B, C, quantification in D–E) and microglia morphology resembles an activated state (Supplementary Fig. 4B, C). We also confirm that deletion of TβRII in CX3CR1+ cells specifically affects downstream signaling in IBA1+ cells and not IBA1- cells indicated by the nuclear localization of pSMAD3 (Supplementary Fig. 4B, C, F–G). Furthermore, loss of type 2 receptor (TβRII) in CX3CR1+ myeloid cells recapitulates the same findings of increased DCX+ cells and dendritic arborization in these *Cx3cr1*^{CreER}-*Tgfbr2*$^{fl/fl}$ iKO mice (Supplementary Fig. 4H–K). In summary, these data suggest that it is not loss of activin, but specifically TGF-β signaling in microglia that mediates the increase in adult SGZ neurogenesis. Next, we also generated *Cx3cr1*^{CreER}-*Tgfb1*$^{fl/fl}$ ligand iKO mice which also recapitulate the same phenotype of

https://doi.org/10.1038/s41467-026-68885-4

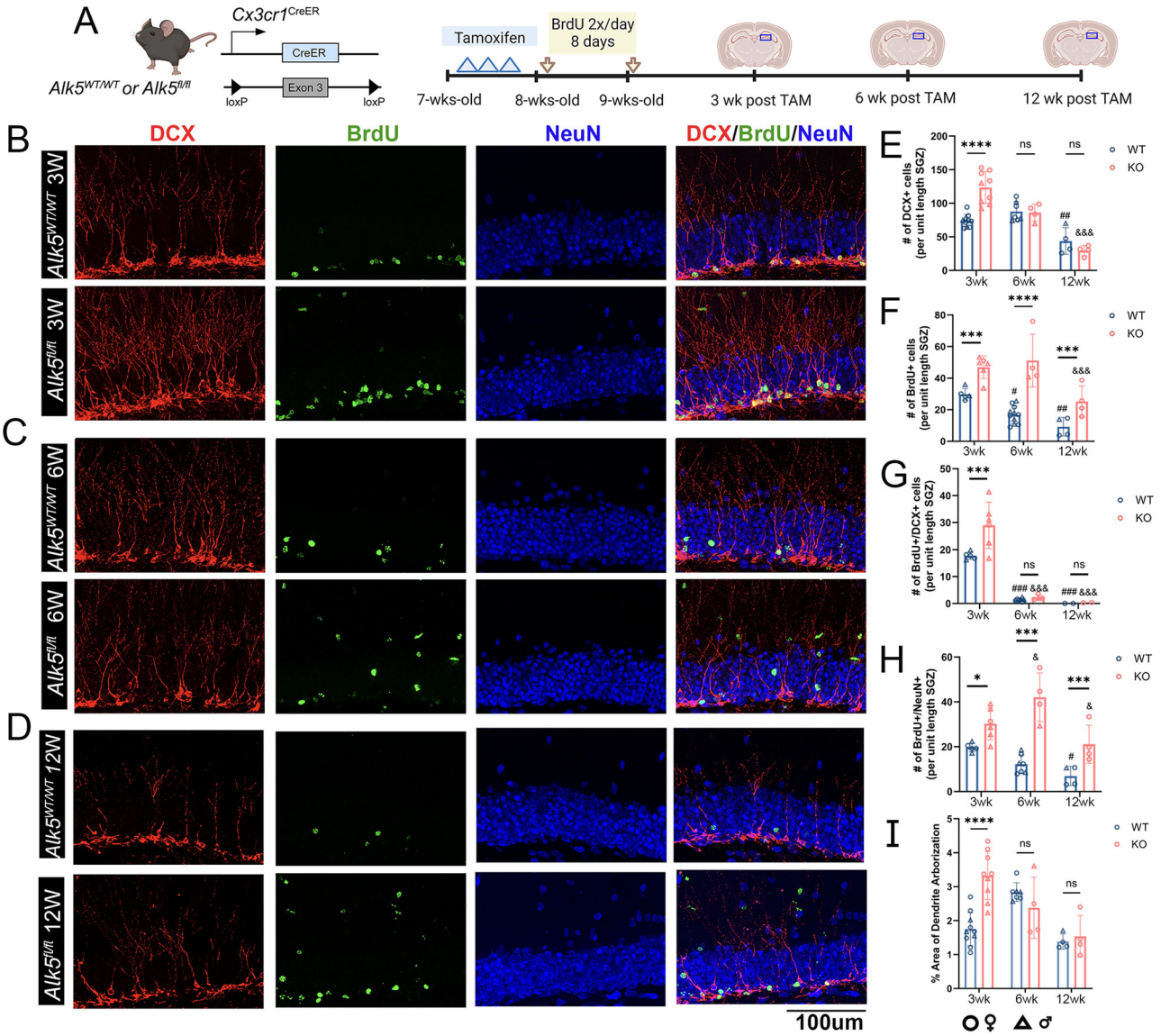

Fig. 2 | *Cx3cr1*^{CreER}*-Alk5 iKO* mice show an increase in a cohort of adult hippocampal neurogenesis. A Mouse model and experimental timeline used to analyze SGZ adult neurogenesis at 3, 6, and 12 weeks post-tamoxifen. Representative images of the hippocampus in *Cx3cr1*^{CreER}*-ALK5*$^{wt/wt}$ and *Cx3cr1*^{CreER}*-ALK5*$^{fl/fl}$ mice at **B** 3 weeks, **C** 6 weeks, and **D** 12 weeks post tamoxifen showing staining for DCX (red), BrdU (green), and NeuN (blue). Quantification for the number of **E** DCX+ cells, **F** BrdU+ cells, **G** BrdU + /DCX+ cells, **H** BrdU + /NeuN+ cells, and **I** dendritic arborization of DCX+ cells at each time point. **E** WT $n = 10, 7, 4$ and KO $n = 9, 4, 4$; **F** WT $n = 5, 11, 4$ and KO $n = 6, 4, 4$; **G** WT $n = 5, 7, 2$ and KO $n = 6, 4, 2$; **H** WT $n = 5, 7, 4$ and KO $n = 6, 4, 2$; **I** WT $n = 10, 7, 4$ and KO $n = 9, 4, 4$. Each data point represents the average of a single animal (3-6 brain sections analyzed per mouse). The sex of each animal is represented by open circles (females) and open triangles (males). **E** (****$p < 0.0001$ (WT v KO 3wk),**$p = 0.007$ (WT 3wk v 12wk), ***$p < 0.001$ (KO 3wk v 12wk) and ns=not significant); **F** (***$p = 0.002$ (WT v KO 3wk), ****$p < 0.0001$ (WT v KO 6wk),***$p = 0.009$ (WT v KO 12wk), *$p = 0.013$ (WT 3wk v 6wk), **$p = 0.002$ (WT 3wk v 12wk), ***$p < 0.001$ (KO 3wk v 12wk)); **G** (***$p < 0.001$ for all comparisons and ns=not significant); **H** (*$p = 0.012$ (WT v KO 3wk), ***$p < 0.001$ (WT v KO 6wk), ***$p = 0.005$ (WT v KO 12wk), *$p = 0.021$ (WT 3wk v 12wk), *$p = 0.017$ (for KO 3wk v 6wk), *$p = 0.038$ (KO 3wk v 12wk)); **I** (****$p < 0.0001$ and ns=not significant). Two-way ANOVA test, two-sided, with Tukey post hoc pairwise comparison was used for statistical analysis in all panels. Mean ± SE. "*" for comparison between WT and KO, "#" indicates significance when compared to 3wk WT group, and "&" indicates significance when compared to 3wk KO group. Scale bar = 100 um. Panel **A** was created in BioRender. Luo, A. (2026) https://BioRender.com/88i2v5l. Source data are provided as a source data file.

increased SGZ adult neurogenesis compared to control mice at 3 weeks post TAM treatment (Supplementary Fig. 5). Additionally, in contrast to the recovery of microglia phenotype in the *Cx3cr1*^{CreER}*-Alk5* $^{fl/fl}$ receptor iKO mice, our results show that *Cx3cr1*^{CreER}*-Tgfb1*$^{fl/fl}$ ligand iKO mice maintain the microglia reactive phenotype and loss of pSMAD3 signal in microglia up to 12 weeks post TAM treatment (Supplementary Fig. 6). Consistent with the sustained microglia reactive phenotype, DCX+ cells remain increased at 12 weeks after TAM treatment in the *Cx3cr1*^{CreER}*-Tgfb1*$^{fl/fl}$ ligand iKO mice (Supplementary Fig. 5). Taken together, our data strongly support that microglia reactivity in the iKO directly contributes to the observed increase in the DCX+ cells in the adult mouse hippocampus.

P2ry12^{CreER} driver line results in deletion of *Alk5* in both microglia and choroid plexus macrophages, which leads to similar increases in immature neurons in the hippocampus as compared to the *Cx3cr1* driver line

We and others have shown that the myeloid-specific driver *Cx3cr1*^{CreER} mouse line targets peripheral monocytes and macrophages in addition to microglia[51,52], which could potentially confound the interpretation

of data regarding microglia-specific mechanisms. While the 3-week timepoint allows for the turnover of circulating monocytes and macrophages via non-recombined CX3CR1-negative bone marrow progenitors, the rapid increase in immature neurons we see at 3 weeks could potentially be attributed to indirect influences from either CNS border-associated macrophages (BAMs) or the transient gene deletion in a cohort of KO monocytes or peripheral tissue-resident macrophages. It has also been reported that the knock-in/knockout *Cx3cr1*^{CreER} mouse lines, where *CreER* is knocked into the *Cx3cr1* locus, disrupt the endogenous *Cx3cr1* gene expression[53,54]. The reduced gene expression of *Cx3cr1* in microglia is reportedly able to modulate adult neurogenesis on its own[55–57] albeit we used the *Cx3cr1*^{CreER}-*Alk5*$^{WT/WT}$ mice as a control to account for this potential caveat. Nevertheless, to circumvent these caveats and to further increase the rigor of our research, we generated the *P2ry12*$^{CreER/CreER}$driver line with the *ALK5*$^{fl/fl}$ line[51] (Fig. 3A). This Cre driver line used a *P2A* sequence to enable *CreER* expression under the control of endogenous *P2ry12* promoter without affecting the expression of endogenous *P2ry12* gene and our previous study showed that homozygous *CreER* in both alleles increased the efficiency of gene deletion in the *Alk5* floxed alleles[51] and can achieve close to 80% reduction in Alk5 gene expression in sorted brain microglia[51]. *P2ry12*$^{CreER/CreER}$-*Alk5*$^{fl/fl}$ mice were treated with TAM following the same paradigm and harvested at 3 weeks post-TAM (Fig. 3A), a time point where we observed the robust increase in the DCX+ cells in SGZ of the *Cx3cr1*^{CreER}-*Alk5*$^{fl/fl}$ mice. Even though there is lower recombination efficiency in *P2ry12*$^{CreER/CreER}$-*Alk5*$^{fl/fl}$ compared to the *Cx3cr1*^{CreER}-*Alk5*$^{fl/fl}$[51], we still observe a significant decrease in immunoreactivity of homeostatic markers *Tmem119* and *P2ry12* in *Alk5* iKO microglia when compared to control (Fig. 3B, C, F–G). Additionally, we show that *Cx3cr1*^{CreER} -*Alk5* iKO mice show loss of pSMAD3 in parenchymal microglia, perivascular macrophages, and choroid plexus macrophages (Supplementary Fig. 7) while *P2ry12*$^{CreER/CreER}$-*Alk5*$^{fl/fl}$ mice show reduced pSMAD3 in parenchymal microglia and choroid plexus macrophages but preserve pSMAD3 in perivascular macrophages (Supplementary Fig. 7). These results are consistent with previous studies showing Cre activity in both microglia and choroid plexus in this mouse line[51,58]. Importantly, the number of DCX+ cells at the SGZ consistently shows an increase in this microglia-specific *P2ry12*$^{CreER/CreER}$-*Alk5*$^{fl/fl}$ mouse model (Fig. 3D, E, H), supporting that reactive microglia and possibly choroid plexus macrophages but not perivascular macrophages or other myeloid cells are responsible for the observed stimulation of adult neurogenesis. Furthermore, we observed increased DCX+ dendritic arborization in the hippocampus of the *P2ry12*$^{CreER/CreER}$-*Alk5*$^{fl/fl}$ mice (Fig. 3D, E, I), consistent with increased DCX+ immature neuron numbers. Taken together, this suggests that *Alk5* deletion in microglia and/or choroid plexus macrophages and the resulting loss of TGF-β signaling in this subset of myeloid cells is sufficient to drive an increase in adult neurogenesis and may, in turn, impact synaptic plasticity and functional outcomes.

Evidence of enhanced survival but not proliferation in the *Cx3cr1*^{CreER}-*Alk5*$^{fl/fl}$ mouse line suggests necessity of microglia to the maturation and survival of adult-born neurons

The increase in immature neurons we observed in various MG-TGF-β signaling-abolished mouse models raises the question of whether alteration in microglia profile modulates adult neurogenesis via enhanced proliferation of NSCs/intermediate progenitor cells (IPCs) or enhanced survival of newly born immature neurons. To test this, we utilized the *Cx3cr1*^{CreER}-*Alk5*$^{fl/fl}$ (Fig. 4A, E) mouse line and either post-labeled (Fig. 4A) or pre-labeled (Fig. 4E) a cohort of newly born cells with BrdU with respect to TAM treatment (induction of gene knockout). The total number of BrdU+ cells at the SGZ line was significantly increased for both pre-and post-labeling paradigms after harvesting mice 3-weeks post TAM (Fig. 4B–H). It is important to note that we are able to analyze these cells by colocalization with either DCX or NeuN but not with IBA1 to identify the adult-born neurons and not proliferating microglia. These data suggest the mechanism of increased DCX+ immature neurons at 3-weeks post TAM and the final mature adult-born neurons (BrdU + /Neun +) 12-weeks post TAM is at least partially increased via survival of newly born cells at the SGZ as tracked in the BrdU pre-labeling paradigm (Fig. 4E–H) because *Alk5* gene knockout was not induced until the newly born cells (BrdU +) were already pre-labeled. This hypothesis is also supported by the increased percentage of BrdU+ cells that survived in the 3-12-week time window in KO vs control mice (50% survived in iKO vs 30% survived in control mice) (Fig. 2). To further test this hypothesis, we further evaluated the number of proliferating cells at 3-,6-, and 12- weeks post TAM with an endogenous cell proliferation marker at the SGZ (quantification is for Ki67 + /IBA1- cells) and found no significant difference between control and *Cx3cr1*^{CreER}-*Alk5*$^{fl/fl}$ mice at any of the time points examined (Supplementary Fig. 8).

Microglia ablation via PLX5622 does not lead to increased SGZ adult neurogenesis but repopulation of CNS with *Alk5* KO microglia after PLX5622 ablation increases adult neurogenesis in the hippocampus

Loss of TGF-β signaling leads to loss of homeostatic signature microglia genes and upregulation of proinflammatory genes such as *Tnf* and genes that stimulate proliferation and cell survival, such as *Igf1*[36]. Microglia have been speculated to regulate adult neurogenesis via their secretome or by phagocytosing of apoptotic newborn cells[28,29]. To investigate whether the observed changes in SGZ adult neurogenesis are due to the loss of a critical homeostatic function of "physiologically normal" microglia, we investigated the SGZ adult neurogenesis in mice that lacked microglia using microglia ablation agent, PLX5622[36]. To label adult neural stem cells and their progeny, we crossed the *Nestin*^{CreER} line[59] with the Ai9 reporter line (Fig. 5A) so that upon TAM administration, we can endogenously track a NSC-specific cohort of adult-born tdTomato+ cells in the SGZ. We treated *Nestin*^{CreER}-*Ai9* mice with TAM and fed the mice either control or PLX5622 diet for 3 weeks (Fig. 5A), a similar timeline to the loss of *Alk5* in microglia in the MG-*Alk5* iKO mice. A significant decrease of Iba1+ cells was observed (Fig. 5B, C, G), indicating successful depletion of microglia in the adult mouse brain. However, we observed no significant difference in the number of tdTomato+ (Fig. 5B–D), DCX+ (Fig. 5B, C, E), or tdTomato + /DCX+ cells (Fig. 5B, C, F), suggesting that the increase in DCX+ cells observed in the *Cx3cr1*^{CreER}-*Alk5*$^{fl/fl}$, *P2ry12*$^{CreER/CreER}$-*Alk5*$^{fl/fl}$, *Cx3cr1*^{CreER}-*Tgfb1*$^{fl/fl}$, and *Cx3cr1*^{CreER}-*Tgfbr2*$^{fl/fl}$ mouse models is not due to a loss of "normal" microglia function. In addition to this, *Cx3cr1*^{CreER}-*Alk5*$^{WT/WT}$ and *Cx3cr1*^{CreER}-*Alk5*$^{fl/fl}$ mice were subjected to a control or PLX5622 diet for 3 weeks and administered TAM post-microglia ablation (Fig. 6A), proceeding the withdrawal of PLX5622 diet to allow the repopulation of these WT or KO microglial cells. Our previous study has shown that repopulating CNS microglia from TGF-β signaling-deficient (via *Alk5* gene knockout) microglia after PLX5622 ablation leads to overpopulation of microglia and repopulation of reactive microglia (Fig. 6 and Bedolla et al.[36]). This experiment allows us to evaluate the effects of repopulating KO microglia on adult SGZ neurogenesis. Repopulated microglia in MG-*Alk5* iKO microglia displayed less ramified morphology and downregulation of homeostatic marker *Tmem119* and increased CD68 expression (Fig. 6B, C, G, H), consistent with our previous report[36]. Importantly, consistent with our previous report[36], TGF-β deficiency in iKO microglia does not lead to acute neurodegeneration in adult mouse brain (evaluated by unbiased stereology counts of all layers of cortical neurons Fig. 6E and Bedolla, et al.[36]). Interestingly, with this treatment paradigm after *Alk5* KO microglia repopulation, the number of immature neurons in the hippocampus was also significantly increased in MG-*Alk5* iKO when compared to the control mice (Fig. 6D, I, J), with a large effect size (Cohen's d = 8.755227 and coefficient r = 0.9748874 for Fig. 6I and

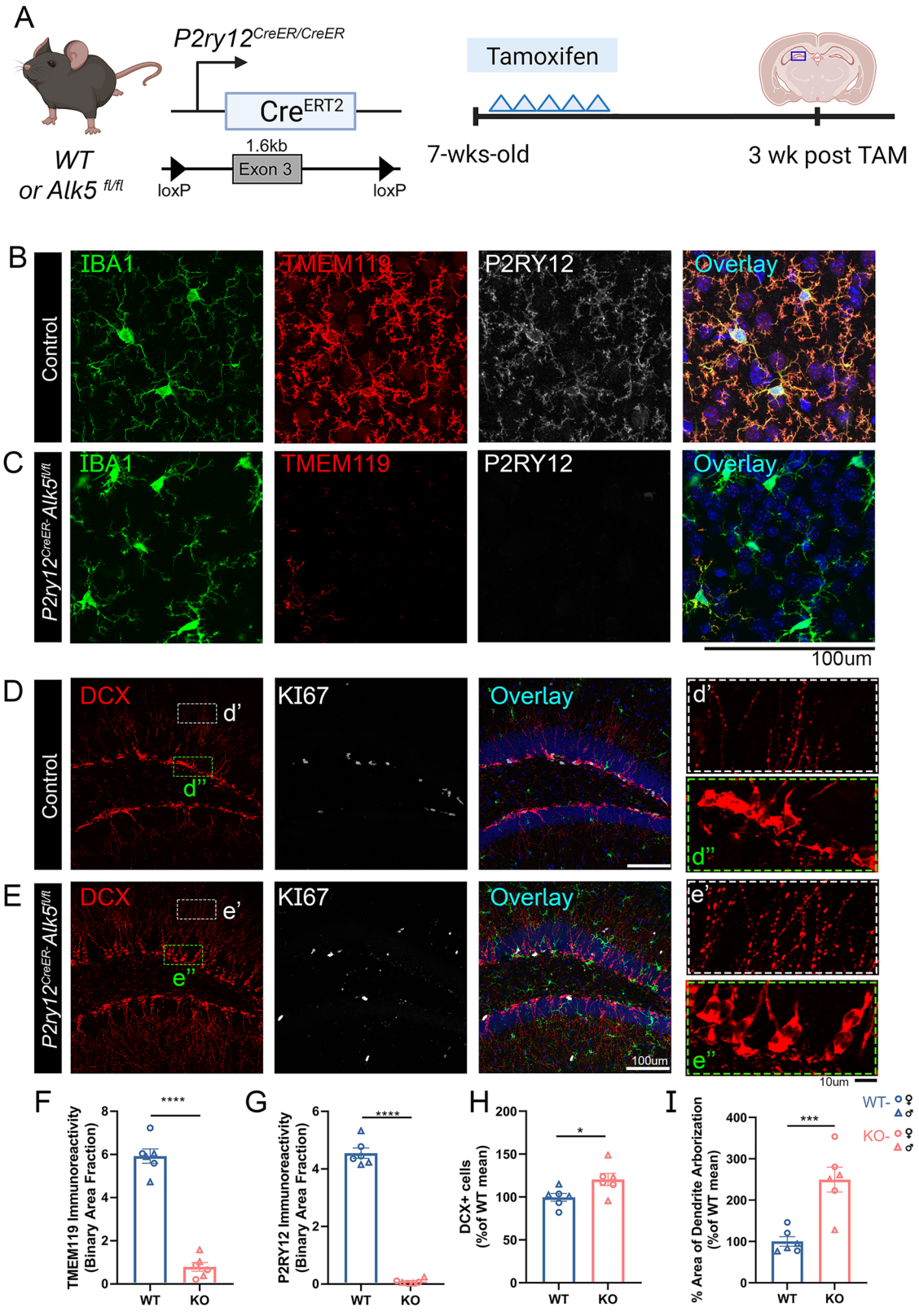

Cohen's d = 5.4435 and coefficient r = 0.9386 for Fig. 6J), albeit a small n number. Taken together, these results suggest that the increased SGZ neurogenesis is not merely due to loss of a "physiologically normal" microglia function, but rather, it suggests that the enhanced neurogenesis in SGZ is likely due to certain gain-of-function mechanisms from the KO microglia that occur after the disruption of Alk5-mediated TGF-β signaling.

Reactive microglia in MG-*Alk5* iKO mice enhance SGZ neurogenesis not by upregulation of microglial *Igf1* or *Tnfa* but by upregulation of epilepsy-related genes and downregulation of PTEN pathway in the neuroblasts at the hippocampus

We next carried out scRNAseq of the dissected whole hippocampus in control, MG-*Tgfb1*, and MG-*Alk5* iKO mice at 3 weeks after TAM treatment (Fig. 7A, B **and** Supplementary Fig. 9 for QC plots) in the presence

Fig. 3 | *Alk5* gene deletion in a P2ry12$^{CreER/CreER}$ driver line results in increased neuroblasts/immature neurons and dendritic arborization in adult SGZ. **A** Mouse model for targeting microglial (*P2ry12*$^{CreER/CreER}$) *Alk5* in adult mice to examine adult neurogenesis in SGZ. **B**–**C** Representative images showing immunohistochemistry staining for IBA1, TMEM119, and P2RY12 (Clone P2YM 1E5) in **B** control mice and **C** *P2ry12*$^{CreER/CreER}$-*Alk5*$^{fl/fl}$ at 3 weeks after TAM administration. **D**, **E** Representative images showing immunohistochemistry staining for DCX and Ki67 in **D** control mice and **E** *P2ry12*$^{CreER/CreER}$-*Alk5*$^{fl/fl}$ at 3 weeks after TAM administration. **F**–**I** Quantification for **F** TMEM119 immunoreactivity, **G** P2RY12 immunoreactivity, **H** DCX+ cells quantification compared to the wildtype mean, and **I** quantification of dendritic arborization (% of immunoreactive positive area) compared to the wildtype mean. **F** ($n = 6$ for WT and $n = 6$ for KO, $^{****}p < 0.0001$); **G** ($n = 6$ for WT and $n = 6$ for KO, $^{****}p < 0.0001$); **H** ($n = 6$ for WT and $n = 6$ for KO, $^{*}p = 0.0359$); **I** ($n = 6$ for WT and $n = 6$ for KO, $^{***}p = 0.0009$). Each data point represents the average of a single animal (3–6 brain sections analyzed per mouse) and $n = 6$ for each group (wildtype or knockout). The sex of each animal is represented by open circles (females) and open triangles (males). Mean ± SE. Two-sided Student's t-test for all panels except Welch's t-test was used for panel G. Scale bar as indicated. Panel **A** was created in BioRender. Luo, A. (2026) https://BioRender.com/1834acf. Source data are provided as a source data file.

of transcription and translation inhibitors[60] to avoid microglia profile changes during tissue collection. ScRNAseq data identified different cell clusters, including microglia and neuroblasts/immature neurons (Fig. 7C). Utilizing known cells markers such as *Aif1* (Fig. 7D) and *Dcx* (Fig. 7E) alongside Cell Marker 2.0 or Allen Cell Types Database, we were able to annotate the clusters and determine cell type for further downstream analysis. The microglia cluster showed enriched signature microglia marker genes, such as *Aif1*(Fig. 7D), *TMEM119, P2ry12* (Fig. 7F and G) but not other cell type markers, such as astrocyte markers *(Aldh1l1* or *Gfap*, Fig. 7H and I). DEG analysis shows differences in the gene expression of 360 genes between MG-*Alk5* iKO vs control (Fig. 7J, see Supplementary Fig. 9 for split UMAP for all three groups and complete DEGs listed in Supplementary Data 1). MG-*Tgfb1* iKO mice showed differences in the gene expression of 327 genes in the microglia cluster (Supplementary Fig. 9F, complete DEGs listed in Supplementary Data 3 and Supplementary Fig. 9H for 141 overlapping genes between *Alk5* and *Tgfb1* iKO microglia DEGs). In the neuroblast cluster, the expression of 2324 genes are altered in the MG-*Alk5* iKO mice (Fig. 7K, complete DEGs listed in Supplementary Data 2) while 2229 genes are altered in the MG-*Tgfb1* iKO (Supplementary Fig. 9G, complete DEGs listed in Supplementary Data 4, with 1779 overlapping of neuroblast DEGs between *Alk5* and *Tgfb1* iKO mice shown in Supplementary Fig. 9I). Interestingly, out of the overlapping neuroblasts DEGs (Supplementary Fig. 9I), GO:BP gene pathway analysis shows upregulation of multiple biological processes related to neurogenesis, neuron development, generation of neurons, neuron projection morphogenesis, neuron projection development, neuron differentiation and synapse organization (Supplementary Fig. 9J, see full list in Supplementary Data 5) which is consistent with the observed phenotype in altered neurogenesis. Biological processes that were downregulated in the Go:BP gene pathway analysis include regulation of cellular process, localization, and establishment of localization (Supplementary Fig. 9K, see full list in Supplementary Data 6), consistent with aberrant neurogenesis. Additionally, our analysis using LIANA revealed strong cell-cell interactions between microglia and endothelial cells and microglia-DCX+ immature neuron population mediated by predicted specific ligand-receptor interactions (Fig. 7L, see full list in Supplementary Data 7). Enricher pathway analysis (Elsevier pathway) of the differentially expressed genes (DEGs) from neuroblasts isolated from both MG-*Alk5* iKO and MG-*Tgfb1* iKO mice identified several overlapping top significantly altered disease-related or cellular processes (Fig. 7M, complete DEGs listed in Supplementary Data 8 for MG-*Tgfb1* iKO) and specific molecular pathways (Fig. 7N) identified from the neuroblasts derived from either MG-*Alk5* iKO or MG-*Tgfb1* mice. Among these, we focused on the TNF-α, IGF-1, and PTEN-PI3K/AKT/mTOR signaling pathways (Fig. 7N). IGF1 has been shown to increase adult neurogenesis[40,61,62] and oligodendrocyte development[63]. Interestingly, our data show that there is also increased OLIGO2+ cells and OLIGO2 + /NG2 + oligodendrocyte progenitor cells (OPCs) in the hippocampus of *MG-Alk5* iKO mice (Supplementary Fig. 10). Peripheral infusion of IGF-1 increased the amount of progenitors present in the GCL[62]. Additionally, increased levels of IGF-1 in the brain have been found after voluntary exercise, an external method commonly used to increase neurogenesis[64]. Interestingly, both *Tgfb1* and *Alk5* gene deletion lead to increased *Igf1* expression in microglia (Fig. 1I and Bedolla et al.[36]). To investigate whether increased *Igf1* growth factor from iKO microglia is responsible for the increased adult neurogenesis in the MG-*Alk5* iKO mice, we generated *Cx3CR1*^{creERT2}-*Alk5* $^{fl/fl}$/*Igf1*$^{fl/fl}$ double knockout mouse model (Fig. 8A). Following a similar experimental timeline, control, *Alk5* single iKO, and *Alk5/Igf1* double iKO mice were harvested at 3 weeks post TAM treatment (Fig. 8A). We compared the *Cx3CR1*^{creERT2}-*Alk5*$^{fl/fl}$/*Igf1*$^{fl/fl}$ model against the *Cx3cr1*^{CreER}-*Alk5*$^{fl/fl}$ model to ensure we had efficient gene deletion of *Alk5* in sorted microglia in both the *Alk5* single iKO and the *Alk5/Igf1* double iKO (dKO) mice (Fig. 8H–J). Additionally, in the *Alk5/Igf1* dKO mice, the upregulation of *Igf1* in microglia is abolished (Fig. 8K). Interestingly, abolishment of *Igf1* gene in the *Alk5/Igf1* dKO mice does not rescue the downregulation of homeostatic markers *Tmem119* and *P2ry12* (Fig. 8B–D). More importantly, despite the successful abolishment of *Igf1* upregulation in the dKO mice, the phenotype of increased adult neurogenesis (measured by increased newly born neuroblasts DCX+ cells and dendritic arborization) remained in the *Alk5/Igf1* dKO mice (Fig. 8E–G, L, M). Despite previous studies reporting the importance of microglial *Igf1* in regulating adult neurogenesis under other contexts and the substantial upregulation of *Igf1* in the *Cx3cr1*^{CreER}-*Alk5*$^{fl/fl}$ mouse model, our data suggests that at least microglial-derived *Igf1* growth factor is not likely the cellular factor that mediate the microglia-NPCs crosstalk in our MG-*Alk5* iKO mouse model. Similarly, TNF-α has been reported to have both pro- and anti-neurogenic effects[34,65], we therefore generated double MG-*Alk5* iKO on a constitutive *Tnfa* KO mouse background (Supplementary Fig. 11) at followed the same experimental paradigm as our single iKO mouse experiment. Again, to our surprise, *Tnf* loss of function did not alter the phenotype of heightened SGZ neurogenesis (measured by total DCX+ cells and DCX+ dendritic arborization) in the MG-*Alk5* iKO/*Tnf* dKO mice (Supplementary Fig. 11), suggesting that upregulated *Tnf* by itself is also not sufficient to explain the phenotype. Previous studies have shown that while blocking of individual cytokines failed to abolish the effects of reactive microglia on stimulating neurogenesis in vitro, combined antibodies that block several of the candidate cytokines had a significant effect, suggesting that synergistic and compensatory effects might be at play between the microglial-NSC crosstalk[66]. Given our negative results targeting individual cytokines and the reports from previous studies mentioned above, we then turned our focus more towards cellular pathways that could potentially have a convergent effect on immature neurons. We next focused on the PTEN-PI3K/AKT/mTOR pathway. Notably, PTEN, a negative regulator of the mTOR pathway, was downregulated among the DEGs of immature neurons (Fig. 7K). Moreover, there was a significant alteration in the PTEN-dependent cell cycle arrest and apoptosis pathway (Fig. 7N). Loss of PTEN function in neurons is known to induce epilepsy and enhance neurogenesis in the adult hippocampus[67]. Downregulation of PTEN could lead to enhanced mTOR signaling, which was one of the identified altered pathways in the neuroblast cluster in the iKO mice (Fig. 7N). This hypothesis is further supported by the significant changes observed in the "Proteins involved in Epilepsy" pathway (Fig. 7M) in both MG-*Alk5* and MG-*Tgfb1* iKO mice. To

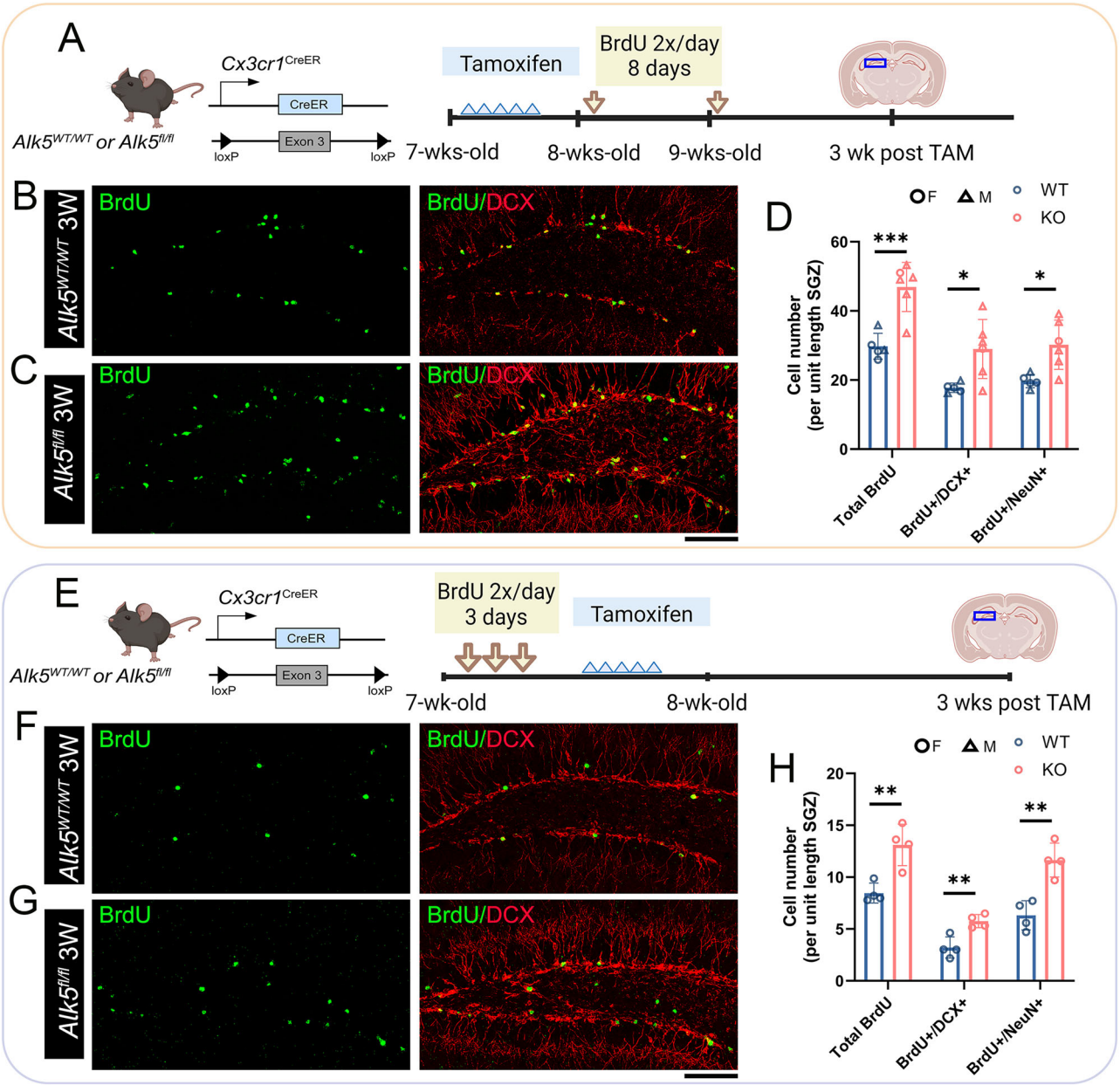

Fig. 4 | Enhanced survival of newly-born adult neurons in the adult mouse hippocampus following microglial deletion of the *Alk5* gene. A Animal model and experimental timeline for post-TAM BrdU labeling. Representative images showing (**B**, **C**) immunohistochemistry staining of BrdU (green) and DCX (red). Quantification of **D** the number of total BrdU + , BrdU + /DCX + , and BrdU + /NeuN+ cells. **E** An experimental timeline for pre-labeling of dividing cells prior to tamoxifen treatment with representative images showing (**F**–**G**) immunohistochemistry staining of BrdU (green) and DCX (red). Quantification of cell number per DG section with regards to **H** total BrdU+ cells, BrdU + /DCX + , and BrdU + /NeuN+ cells. **D** ($n = 5$ for WT and $n = 6$ for KO, $^{***}p = 0.0009$ (for Total BrdU), $^{*}p = 0.180$ (for BrdU + /DCX +), and $^{*}p = 0.0111$ (for BrdU + /Neu*N* +)); **H** ($n = 4$ for WT and $n = 4$ for KO, $^{**}p = 0.0057$ (for Total BrdU), $^{**}p = 0.0055$ (for BrdU + /DCX +), and $^{**}p = 0.0026$ (for BrdU + /Neu*N* +)). Each data point represents the average of a single animal (3–6 brain sections per mouse). The sex of each animal is represented by open circles (females) and open triangles (males). Mean ± SE. Two-sided Student's t-test for all panels and groups except Welch's t-test was used for panel **D** BrdU + /DCX+ group. Scale bar = 100 μm. Panel **A** and **E** was created in BioRender. Luo, A. (2026) https://BioRender.com/uxqbssx. Source data are provided as a source data file.

test whether a TGF-β-deficient microglia profile in the MG-*Alk5* iKO mice enhances SGZ neurogenesis by downregulation of PTEN and upregulation of mTOR pathway, we treated the MG-*Alk5* iKO mice with rapamycin daily, a well-characterized mTOR inhibitor starting from 4 days after TAM administration (Fig. 9A, B) and harvested mice 3 weeks after TAM administration. Interestingly, Rapamycin treatment reversed the phenotype of increased DCX+ immature neurons and increased dendritic arborization in SGZ of the MG-*Alk5* iKO mice (Fig. 9C–F) while having no effects on the total DCX+ cell number in WT mice (Fig. 9C–F). Similarly, dendritic arborization of DCX+ immature neurons was decreased following rapamycin treatment in MG-*Alk5* iKO but not in WT mice (Fig. 9C–F). Additionally, rapamycin-treated WT and MG-*Alk5* iKO both show the ectopic location of DCX+ neuroblasts cells in the outer layer of GCL (Fig. 9C–F) compared to vehicle-treated mice, suggesting either delayed maturation and failure to downregulate DCX in migrated newly-born neurons or enhanced ectopic migration of DCX+ neuroblasts in the GCL by rapamycin treatment. To examine whether MG-*Alk5* results in mTOR pathway

https://doi.org/10.1038/s41467-026-68885-4

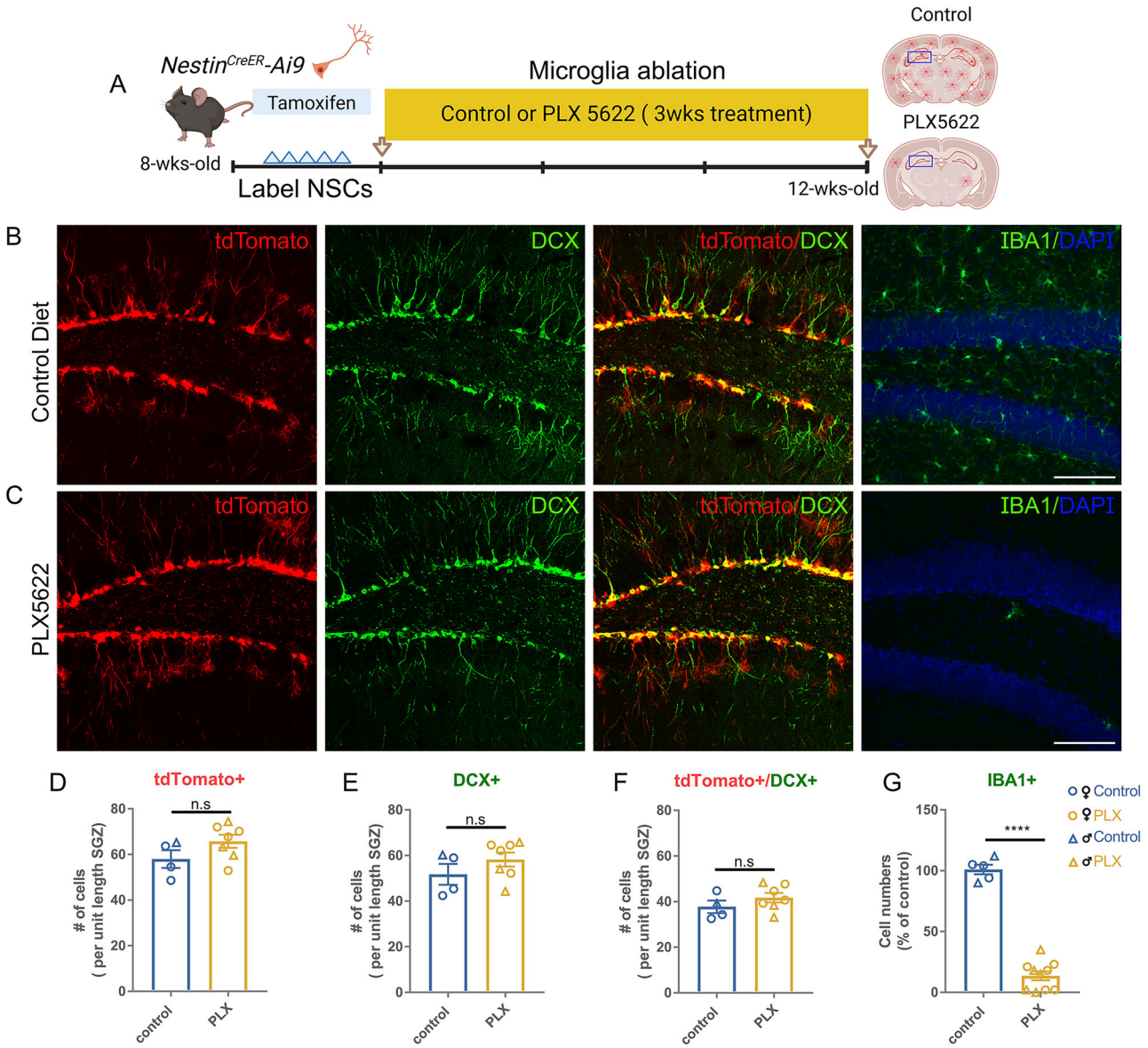

Fig. 5 | Microglia ablation via PLX5622 does not lead to increased SGZ adult neurogenesis. A Neural stem cell-specific mouse model genetically labeling adult-born neurons to examine the effects of microglial ablation on DCX+ cells (**B**, **C**). Representative images showing tdTomato, DCX, and IBA1 expression in **B** *Nestin*^{CreER}-Ai9 (tdTomato) reporter mice given a control diet or **C** PLX5622 diet. **D**–**G** Quantification for **D** the number of tdTomato+ cells **E** DCX+ cells **F** the colocalization of tdTomato + /DCX+ cells in the SGZ, and **G** the number of IBA1+ cells in control or PLX5622 treated mice. **D** ($n = 4$ for control and $n = 6$ for PLX, ns = not significant); **E** ($n = 4$ for control and $n = 6$ for PLX, ns = not significant); **F** ($n = 4$ for control and $n = 6$ for PLX, ns= not significant); **G** ($n = 5$ for control and $n = 10$ for PLX, ****$p < 0.001$). Each data point represents the average of a single animal (3–6 brain sections per mouse). The sex of each animal is represented by open circles (females) and open triangles (males). Mean ± SE. Two-sided Student's t-test was used for all panels. Scale bar = 100 μm. Panel **A** was created in BioRender. Luo, A. (2026) https://BioRender.com/k88gw1g. Source data are provided as a source data file.

upregulation in vivo in SGZ neuroblasts in vivo, we analyzed phosphorylated S6 protein (pS6) as a downstream target for the mTOR pathway specifically in DCX+ immature neuroblasts. pS6 levels in DCX + cells increased in MG-*Alk5* iKO SGZ, which is abolished by rapamycin treatment (Fig. 9H and G). Because both DCX+ cells and OPCs increased in the *MG-Alk5* iKO mice at 3 weeks post TAM, to further investigate whether microglia directly interact with NSCs during neuronal differentiation, we examined WT primary adult NSCs in 3D neurosphere differentiation when they are co-cultured with either WT or Alk5 KO primary microglia (Fig. 9I and J). When NSCs undergo neuronal differentiation (induced by growth factor withdrawal), compared to those co-cultured with WT microglia, NSCs co-culture with the *Alk5* KO microglia show increased neuronal differentiation, measured by TUJI immunoreactivity (Fig. 9K, L). Similar to our in vivo data, rapamycin treatment rescued this phenotype (Fig. 9K, L), supporting a direct interaction of reactive microglia with adult NSCs during differentiation. To further examine whether rapamycin itself blocks the reactivity of microglia in *Alk5* iKO mice, we also evaluated the morphology of *Alk5* iKO microglia in either the vehicle- or rapamycin-treated group and found similar reactivity index quantified by the total length of processes, ramification index, and the area covered by individual microglia processes. Rapamycin treatment does not block the reactivity of microglia in the MG-*Alk5* iKO mice, nor does it affect the morphology of microglia in WT mice (Supplementary Fig. 12). Taken together, our data support a PTEN-mTOR axis that could mediate enhanced adult SGZ neurogenesis caused by reactivity in microglia due to silencing of TGF-β signaling (Fig. 9M).

https://doi.org/10.1038/s41467-026-68885-4

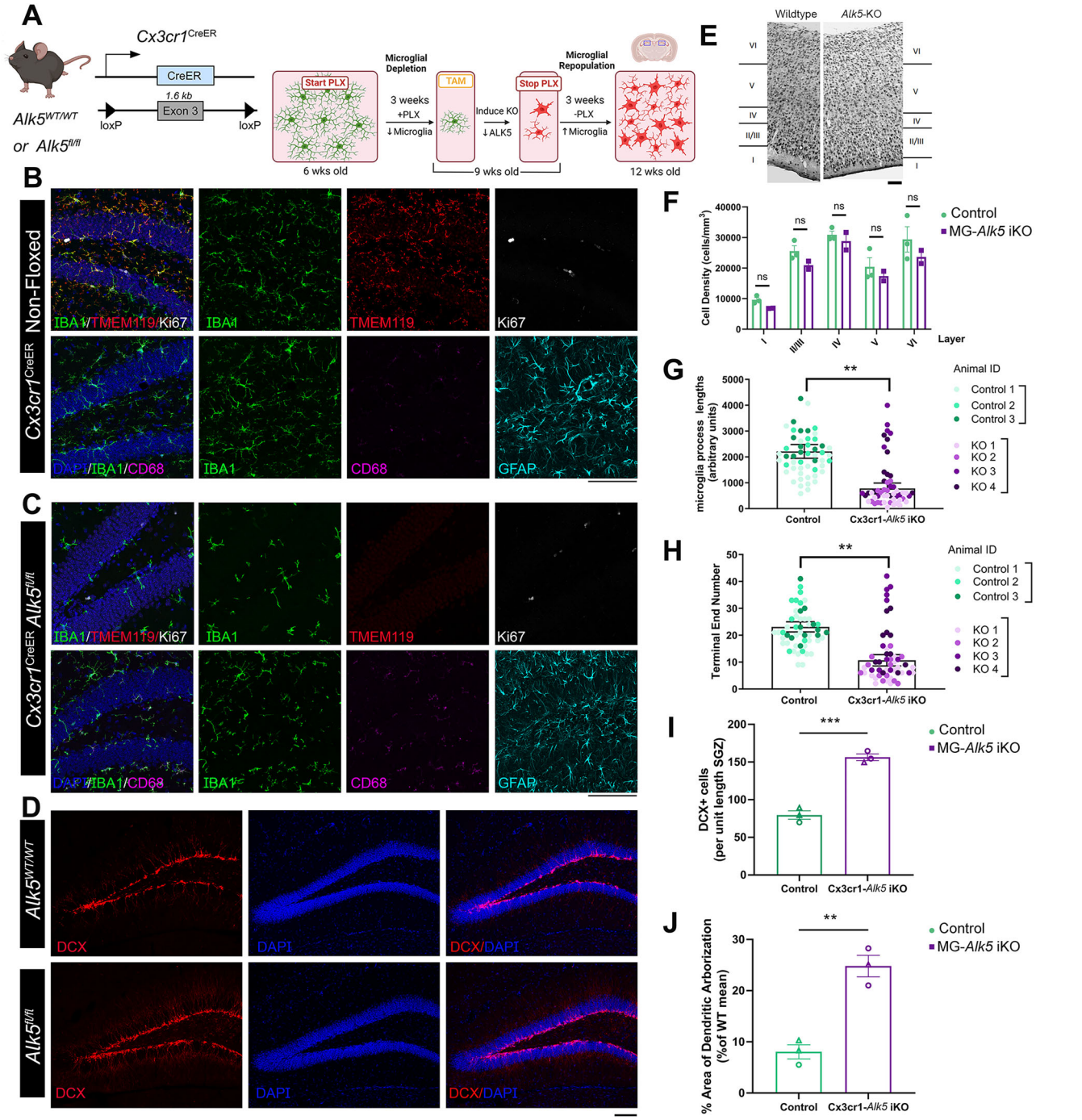

Fig. 6 | Loss of TGF-β signaling via ALK5-dependent signaling in microglia leads to increased neuroblasts in the SGZ during the repopulation of microglia after PLX5622 ablation. A Animal model and Experimental timeline illustrating *Alk5* gene deletion repopulating microglia after PLX5622 ablation. Representative images of **B** *Cx3cr1*^{CreER}-*ALK5*$^{WT/WT}$ or **C** *Cx3cr1*^{CreER}-*ALK5*$^{fl/fl}$ showing immunohistochemistry staining for IBA1, Tmem119, Ki67, CD68, and GFAP after 3 weeks of repopulation post PLX 5622 treatment. **D** *Cx3cr1*^{CreER}-*ALK5*$^{WT/WT}$ or *Cx3cr1*^{CreER}-*ALK5*$^{fl/fl}$ representative images showing DCX (red) and DAPI (blue) at SGZ. **E** Representative image of NeuN staining in the cortex and unbiased stereological quantification of **F** neuronal cell density in each layer, **G** microglia process length, **H** terminal end number, **I** the number of DCX+ cells, and **J** dendritic arborization in the hippocampus. **F** ($n = 3$ for control and $n = 2$ for KO, ns= not significant); **G** ($n = 3$ for control and $n = 4$ for KO, $^{**}p = 0.01$); **H** ($n = 3$ for control and $n = 4$ for KO, $^{**}p = 0.0072$); **I** ($n = 3$ for control and $n = 3$ for KO, $^{***}p = 0.0004$); **J** ($n = 3$ for control and $n = 4$ for KO, $^{**}p = 0.0026$). Each data point in panel (**G**, **H**) represents one cell, and each cell is color-coded to match the animal it came from (statistical analysis is carried out by averaging all cells from the same animal as a single n, with $n = 3$ mice for WT and $n = 4$ mice for KO). Each data point for **I**, **J** represents the average of a single animal (3–6 brain sections per mouse). The sex of each animal is represented by open circles (females) and open triangles (males). Mean ± SE. Two-sided Student's t-test was used for statistical analysis for all panels. Scale bar = 100 μm. Panel **A** was created in BioRender. Luo, A. (2026) https://BioRender.com/j7hbkna. Source data are provided as a source data file.

https://doi.org/10.1038/s41467-026-68885-4

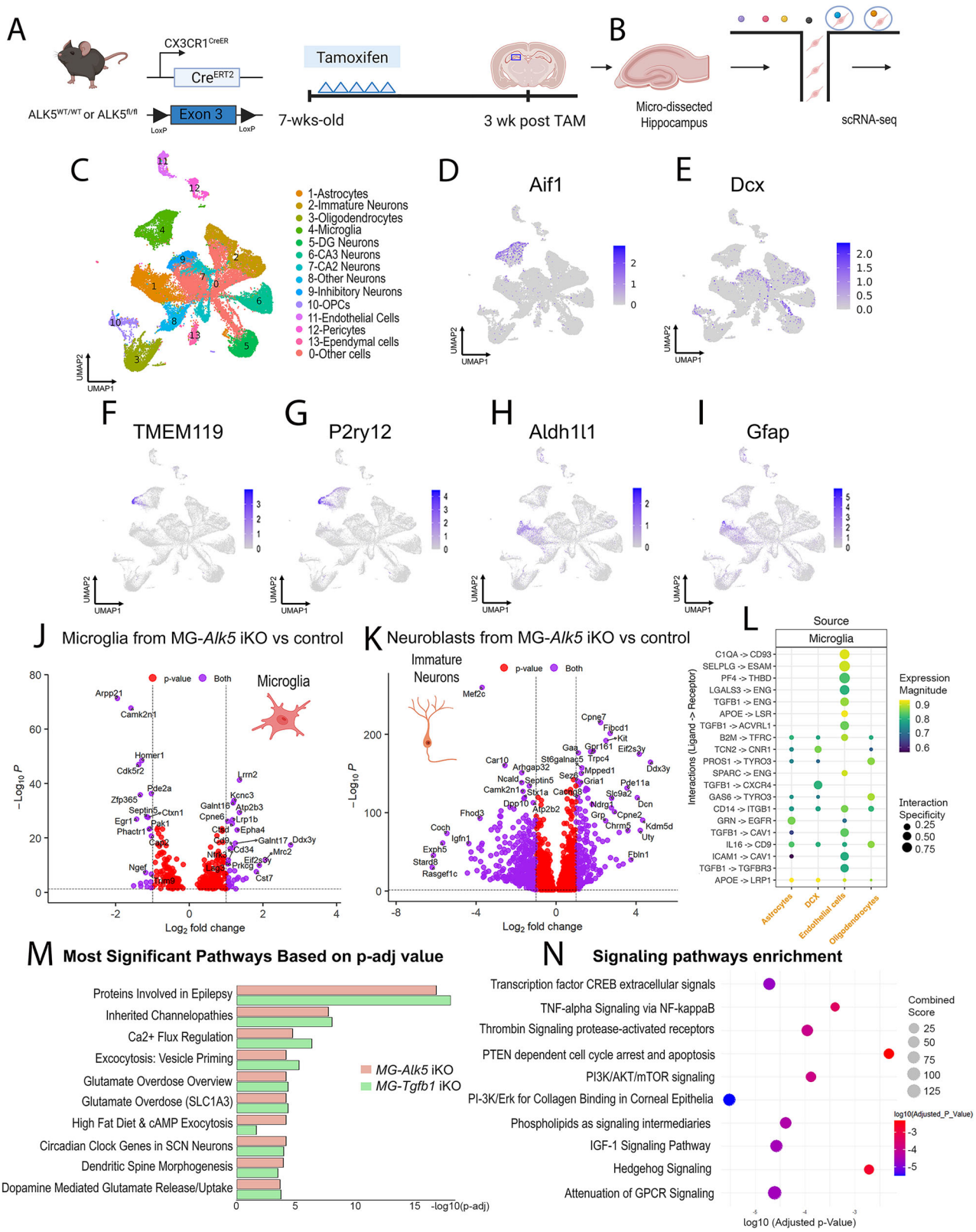

Disruption of microglial TGF-β signaling decreases anxiety-like behavior in Elevated Plus maze that corresponds to microglia status

Next, we sought to further explore our findings related to the increased survival of these newly-born neurons and how their integration into the neural circuitry may impact behavioral functions. Given that the receptor (*Alk5*) and ligand (*Tgfb1*) iKO mice show different properties in the recovery of microglia homeostasis after TAM-induced gene deletion in microglia, we are especially interested in whether the behavioral phenotypes mirror the temporal pattern of changes in adult hippocampal neurogenesis in these two different mouse lines. First, we examine the behavioral phenotype in the MG-Alk5 iKO mice. *Cx3cr1*^{CreER}-*Alk5*$^{WT/WT}$ or *Cx3cr1*^{CreER}-*Alk5*$^{fl/fl}$ mice (Fig. 10A) were subjected to behavioral assessments at 7-8 weeks

Fig. 7 | ScRNAseq analysis of the dissected hippocampus from control, MG-*Alk5* or *Tgfb1* iKO mice show microglia-neuroblasts crosstalk and identifies IGF-1, TNF-α, PTEN/mTOR pathways as mediators for the increased neurogenesis in the iKO mice. A mouse model used to **B** micro-dissect the hippocampus and process for single cell 10x Genomic Flex sequencing. **C** UMAP clustering of cells with annotation for immature neurons and microglia. **D** Feature plot of *Aif1* (coding IBA1 protein) marker to denote microglia cluster. **E** Feature plot of *Dcx* to denote DCX+ immature neuroblasts/neuron cluster. **F**–**I** Feature plots of *Tmem119, P2ry12, Aldh1l1* and *Gfap* to denote enrichment of microglial signature genes but not astrocytic signature genes in the microglia cluster. **J** DEGs in MG-*Alk5* iKO derived microglia compared to control microglia presented as a volcano plot. **K** DEGs in MG-*Alk5* iKO derived neuroblasts compared to control neuroblasts presented as a volcano plot. **L** LIANA was used to identify cell-cell interactions and show strong interaction between microglia-endothelial cells and microglia-neuroblasts with identified potential ligand-receptor pairs. **M**, **N** EnrichR pathway analysis of DEGs from neuroblasts in MG-*Alk5* or *Tgfb1* iKO mice with tables denoting top altered disease/cellular processes and molecular pathways. (DEGs) *p* values were calculated using the Wald test with adjustments for multiple comparisons corrected using the Benjamini-Hochberg method, and (GO Process) *p* values were calculated using Fisher's Exact test with adjustments for multiple comparisons were made using Benjamini-Hochberg method. Panel **A** and **B** was created in BioRender. Luo, A. (2026) https://BioRender.com/10eqn6o. Source data are provided as a source data file.

post TAM administration (Fig. 10A) to allow sufficient maturity and integration of adult-born SGZ neurons into the circuitry. Notably, there were no motor deficits seen in these young adult mice (Fig. 10) as previously reported by us in the ablation of microglial TGF-β1 ligand in young adult mice[36]. Adult-born neurons have been implicated in behavioral functions such as anxiety-like and depressive-like behaviors[17]. Given the observed increases in a cohort of adult-born neurons in the SGZ of the MG-*Alk5* iKO mice, we tested the *Cx3cr1*^{CreER}-*Alk5*$^{fl/fl}$ or *Cx3cr1*^{CreER}-*Alk5*$^{WT/WT}$ control mice in an Elevated Plus maze (EPM, Fig. 10B, C). Interestingly, we did observe both increased time and distance in the open arm of the EPM test, suggesting decreased anxiety-like behavior. Alternatively, this could also be attributed to decreased inhibition in exploratory activities in mice, similar to the behavioral phenotypes observed in multiple Alzheimer's disease models[68,69]. In addition to affective functional dysregulation, we also observed spatial memory and learning deficits during the Barnes maze test (Fig. 10F, G) with mild adverse cues (bright light and fan above the maze) to motivate learning. Notably, in the *MG-Alk5* iKO mice, the increase in DCX+ neuroblasts returns to baseline levels at 6-12 weeks after TAM. Additionally, adult-born neurons are reported to show a critical time window when their plasticity (measured by long term potentiation- LTP) is increased[70]. We next investigate whether the phenotype in EPM and BM in the *MG-Alk5* iKO mice persists or recovers with microglial profile recovery at 12 weeks post TAM, when there is no longer an increase in DCX+ cells or when the critical window for the increased plasticity has passed for the cohort of newly integrated neurons. For the 12-week time point, we used Elevated Zero Maze (EZM) instead of EPM to avoid repeated exposure to the same maze, as anxiety-like or passive avoidance behavior is sensitive to such repetition[71,72]. Both phenotypes in the elevated maze and the BM returned to control levels at 12 weeks post TAM injection in the *MG-Alk5 iKO* mice. (Fig. 10D, E, G).

Next, we examine the behavioral phenotype in the *MG-Tgfb1* iKO, in which microglia reactivity persists and the adult hippocampus shows a sustained increase in DCX+ cells both at 3 weeks and at 12 weeks after TAM treatment. In young adult iKO mice, similar to the MG-*Alk5* iKO, general motor learning is not affected as measured by the accelerating speed rotarod test (Fig. 10P). *Cx3cr1*^{CreER}-*Tgfb1*$^{fl/fl}$ iKO mice showed similar increased activity in the open arm of EPM at 6 weeks post TAM (Fig. 10I–K) and learning/memory deficit in the Barnes maze, as previously reported by our study[36] (Fig. 10N). At 12 weeks post TAM, MG-*Tgfb1* iKO mice show a consistent increase in time and distance spent in the open arm in the EZM and deficits in the BM, consistent with the sustained microglia reactivity and increased DCX+ cells in this line. These recapitulated behavioral deficits in learning/memory and altered anxiety-like behavior from both the *Cx3cr1*^{CreER}-*Alk5*$^{fl/fl}$ and *Cx3cr1*^{CreER}-*Tgfb1*$^{fl/fl}$ mice, which correspond to the microglial and adult neurogenesis status, provide further support for the functional consequences of impaired microglial TGF-β signaling in the regulation of adult neurogenesis and neuronal functions.

Discussion

Adult SGZ neurogenesis is an important biological process that has recently been implicated in multiple neurological functions, such as learning and memory, pattern separation, affective behavior, and forgetting[9,73–75]. The SGZ, a neurogenic niche in the hippocampus central to learning and memory, is a key site for this process and allows the addition of new information and plasticity in an overall stable neural network[76]. Therefore, adult neurogenesis is believed to play a critical role in modulating neuroplasticity- the brain's ability to adapt, learn, and repair[10,73,77,78]. Understanding intrinsic as well as extrinsic factors that modulate adult neurogenesis can enhance our knowledge of neuroplasticity and inform strategies to support the beneficial or inhibit the aberrant detrimental neurogenesis.

Microglia have been proposed as a potential key regulator of neurogenesis during early postnatal development and adult neurogenesis at the SVZ[24–28,35]. Microglia ablation in adult mouse brain does not alter the number of proliferating or DCX+ cells at SVZ at 14 days post ablation; however, it reduced the migration of newly born neurons to OB[24]. Additionally, microglia ablation also results in smaller spines in adult-born neurons in the OB and subsequent weaker excitatory synaptic inputs and reduced odor responses[25]. These previous studies support that microglia can modulate SVZ adult neurogenesis, which can lead to altered olfactory function. In contrast, the role of microglia in SGZ neurogenesis is less well understood. Evidence that supports a role of SGZ microglia includes loss of function in *Cx3cr1* and *P2ry12* (which are both microglia-specific homeostatic signature genes) in mice, resulting in reduced SGZ adult neurogenesis under physiological conditions[56] or in epilepsy-induced neurogenesis[35]. Microglia have also been shown to phagocytose apoptotic cells[29] and in turn, could regulate SGZ neurogenesis through their phagocytosis-induced secretome[28]. However, the underlying mechanisms of cell-cell interactions and the molecular pathways modulated in the neurogenic cascade and the functional relevance of such interactions between microglia and SGZ neurogenesis are largely unexplored.

Two main challenges hinder the investigation in this line of inquiry: First, ablation studies, although powerful and providing valuable information on the overall role of microglia in a biological process, by completely removing microglia cells, could potentially abolish both pro and anti-neurogenic mechanisms simultaneously, making it challenging to interpret study results and dissect specific pathways in microglia. Additionally, although many conditions can stimulate neuroinflammation such as CNS injury or neurodegenerative conditions, these are also accompanied by neuronal loss or other changes which could also directly affect neurogenesis[79,80], making it difficult to dissect out the specific and causal role of microglia profile in regulation of neurogenesis. In an effort to overcome these challenges, in this study, we built on our recent findings that abolishing TGF-β signaling in adult microglia causes a profile that resembles a reactive microglia profile without acute neuronal loss[36] in young adult mice, at least during the time frame we are focusing on. This allows us to specifically evaluate the role of reactivity in microglia following loss

https://doi.org/10.1038/s41467-026-68885-4

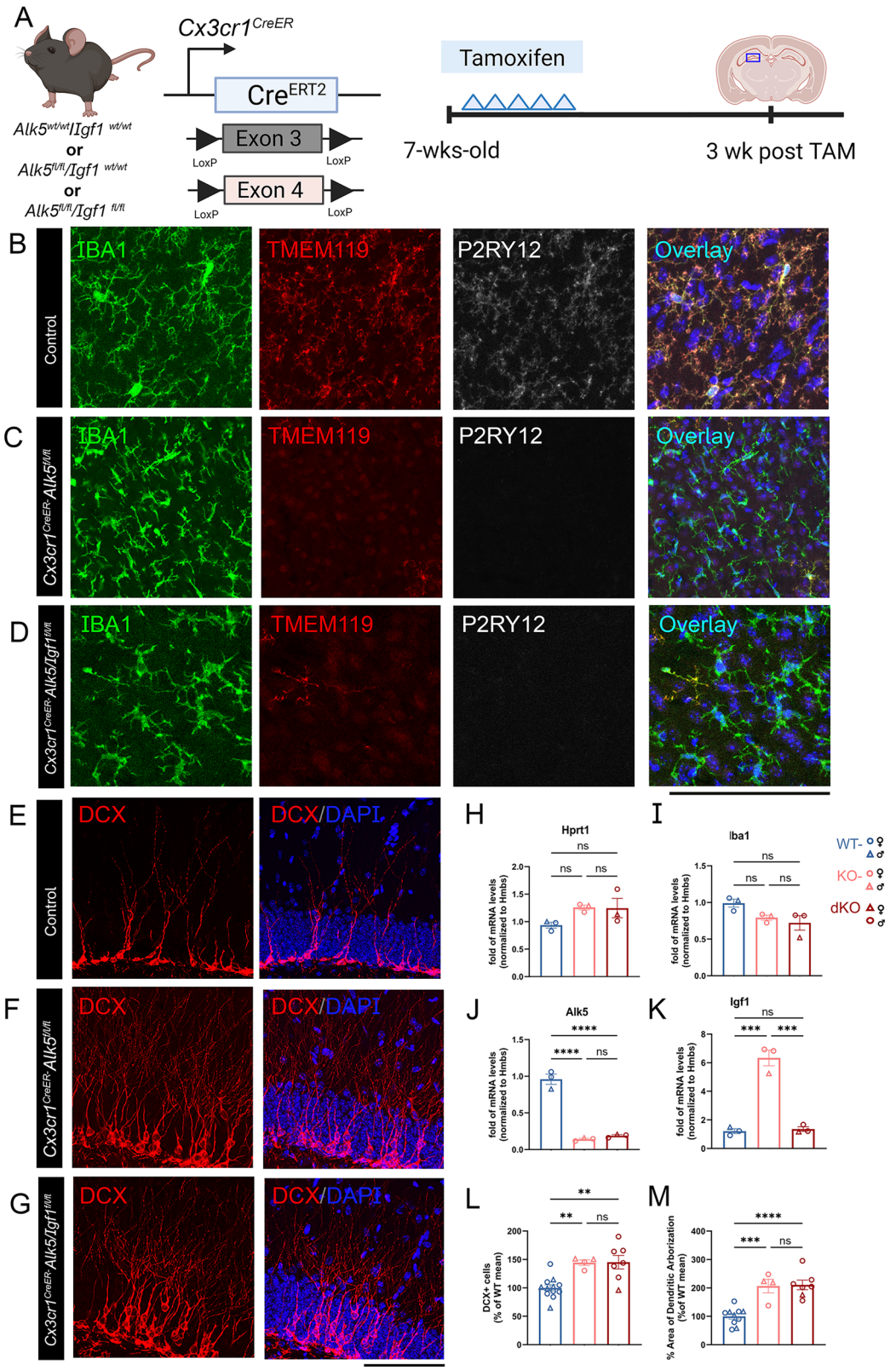

of TGF-β signaling in adult neurogenesis. TGF-β signaling is altered in multiple pathological conditions such as aging, Alzheimer's disease (AD), and CNS injury[81–85], which makes it relevant to a broad range of neurological and pathological conditions.

Contrary to the prevailing understanding[79,86] that neuroinflammation in general is detrimental to neurogenesis, using the inducible KO system specifically targeting microglia and inducing a reactive microglia profile in the adult mouse brain after the development period, our data show surprisingly that loss of homeostatic profiles and gain of a "TGF-β-deficient" microglia profile could transiently stimulate SGZ neurogenesis, which is not only evidenced by increased DCX+ immature neuroblasts at 3 weeks after microglial silencing of TGF-β signaling, but also demonstrated by an increased number of a cohort of newly born BrdU + /NeuN+ neurons at 6 and 12 weeks after TAM

https://doi.org/10.1038/s41467-026-68885-4

Fig. 8 | Microglial-derived IGF1 is not required for the increase in immature neurons present in the hippocampus after deletion of the *Alk5* gene. A The mouse model for single *Alk5* iKO or double *Alk5/Igf1* iKO and experimental timeline (right) for targeting microglial *Igf1* and/or *Alk5* and analyzing immature neurons 3 weeks post tamoxifen. Representative images of immunohistochemistry staining of the hippocampus from tamoxifen-treated (3 weeks post) **A** *Cx3Cr1*$^{CreER(WT/WT)}$, **B** *Cx3Cr1*^{CreER}-*Igf1*$^{fl/fl}$, **C** *Cx3Cr1*^{CreER}-*Alk5*$^{fl/fl}$, **D** *Cx3CR1*^{CreERT2}-*Alk5*$^{fl/fl}$/*Igf1*$^{fl/fl}$ tissue showing IBA1, TMEM119, P2RY12 (P2YM 1E5) staining. **E**–**G** Representative DCX staining in SGZ in above mouse lines. Quantification of mRNA levels from *Cx3Cr1*$^{CreER(WT/WT)}$, *Cx3Cr1*^{CreER}-*Alk5*$^{fl/fl}$, or *Cx3CR1*^{CreERT2}-*Alk5*$^{fl/fl}$/*Igf1*$^{fl/fl}$ sorted microglia (normalized to Hmbs1) showing levels of **H** *Hprt1*, **I** *Iba1*, **J** *Alk5*, and **K** *Igf1* relative to *Cx3Cr1*$^{CreER(WT/WT)}$ mice($n = 3$ for all groups in panels (**H**–**K**)) (ns=not significant (**H**–**I**); **** $p < 0.0001$ and ns=not significant **J**; *** $p = 0.0001$ and $p = 0.0001$ and ns=not significant **K**). **L** Quantification of the number of DCX+ cells and **M** dendritic arborization of DCX+ cells compared to WT mean ($n = 12$ for WT, 4 for *Alk5* KO, and 7 for *Igf1*/*Alk5* KO **L**; $n = 10$ for WT, 4 for *Alk5* KO, and 7 for *Igf1*/*Alk5* KO **M**) (** $p = 0.0071$ and $p = 0.0011$ and ns=not significant for panel **L**; **** $p < 0.0001$ *** $p = 0.0005$ and ns=not significant **M**). The sex of each animal is represented by open circles (females) and open triangles (males). Mean ± SE. One-way ANOVA, two-sided, with Tukey post hoc pairwise comparison was used for statistical analysis in all panels (**H**–M). Scale bar = 100 μm. Panel **A** was created in BioRender. Luo, A. (2026) https://BioRender.com/egkiitm. Source data are provided as a source data file.

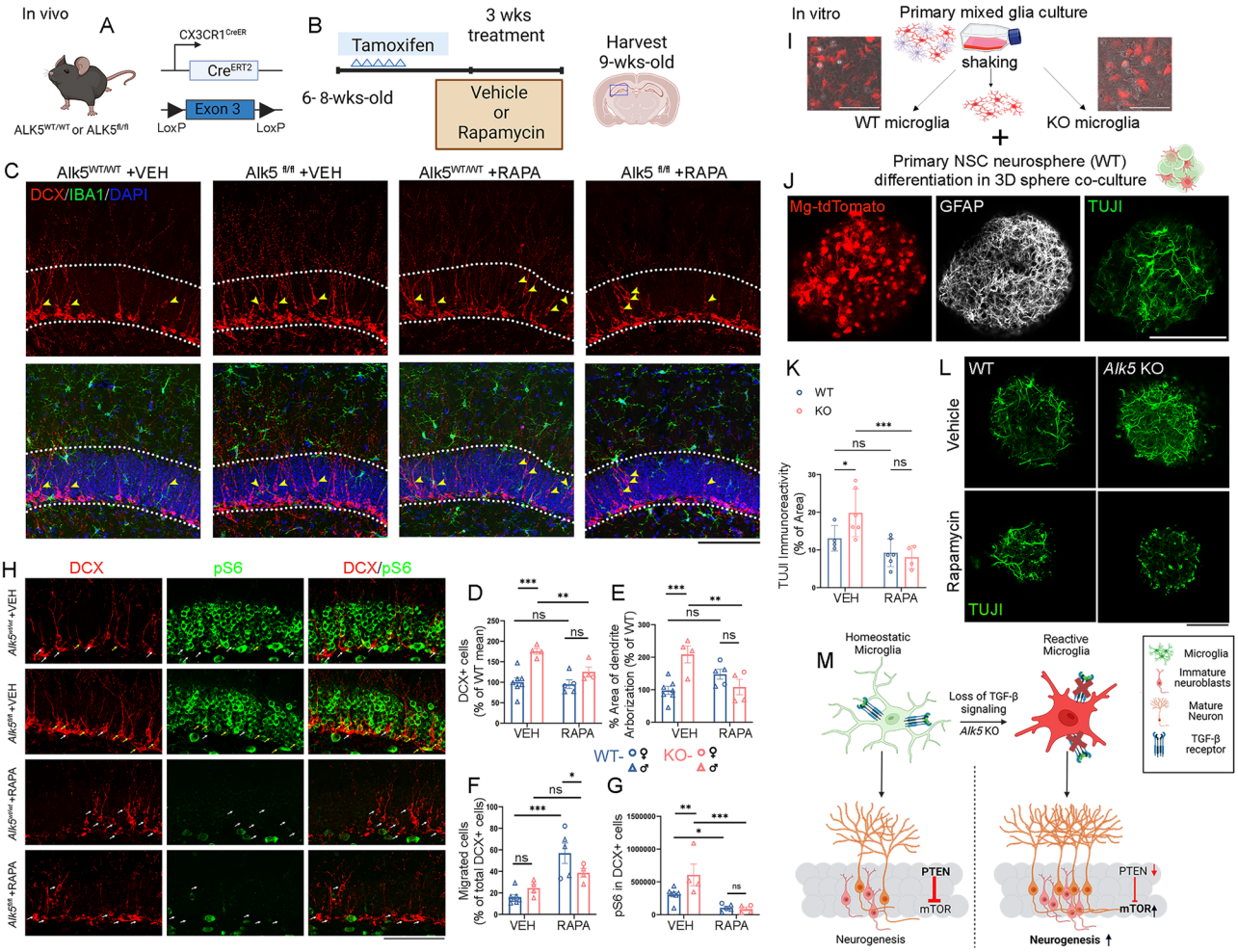

Fig. 9 | In vivo and in vitro functional validation of the downregulated PTEN pathway and upregulated mTOR pathway as key pathway mediating the increased neurogenesis in the *MG-Alk5* iKO mice. A, **B** In vivo animal models used and experimental timeline. **C** Representative images of *Cx3cr1*^{CreER}-*ALK5*$^{WT/WT}$ or *Cx3cr1*^{CreER}-*ALK5*$^{fl/fl}$ treated with either Vehicle (VEH) or Rapamycin (RAPA) showing immunohistochemistry staining for DCX and IBA1 3 weeks after Tamoxifen treatment. Yellow Arrowhead shows DCX+ cells migrated out of the SGZ inner layer. **D** Percentage of total DCX+ cells compared to the wildtype mean and **E** percentage area of dendritic arborization compared to the wildtype mean. **F** Percentage of migrated DCX+ cells relative to the total number of DCX+ cells per mouse. **G**, **H** Representative images of WT or iKO mice treated with either VEH or RAPA showing immunohistochemistry staining for DCX and pS6 3 weeks after TAM treatment. **D**–**G** WT VEH $n = 7$, KO VEH $n = 4$, WT RAPA $n = 5$, and KO RAPA $n = 4$ (ns=not significant (**D**–**G**); *** $p < 0.001$, ** $p = 0.01$ **D**; ** $p = 0.003$, *** $p < 0.001$ **E**; * $p = 0.042$, *** $p < 0.001$ **F**; * $p = 0.048$, ** $p = 0.01$, *** $p < 0.001$ **G**). The sex of each animal is represented by open circles (females) and open triangles (males). **I** In vitro experimental model and timeline for primary adult NSCs and microglia (*P2ry12*$^{CreER/CreER}$-tdTomato) 3D co-culture. **J** Representative images of a differentiated neuroimmune 3D coculture sphere showing microglial tdTomato, GFAP and TUJI immunostaining (maximum projection from Z stacked confocal images). **K**,**L** Representative images of the 3D coculture spheres quantification of the TUJI immunoreactive density in the spheres after differentiation with indicated microglia genotypes and VEH or RAPA treatment (WT VEH $n = 4$, iKO VEH $n = 6$, WT RAPA $n = 6$, iKO RAPA $n = 4$) (ns=not significant, * $p = 0.0352$, *** $p = 0.001$ **K**). **M** A proposed model of mechanistic action through microglia onto adult-born neurons. Mean ± SE. Scale bar = 100 μm, Two-way ANOVA test, two-sided, with Tukey post hoc pairwise comparison was used for statistical analysis for all panels. Panel **A**, **B**,**I** and **M** were created in BioRender. Luo, A. (2026) https://BioRender.com/sxk2w6x. Source data are provided as a source data file.

https://doi.org/10.1038/s41467-026-68885-4

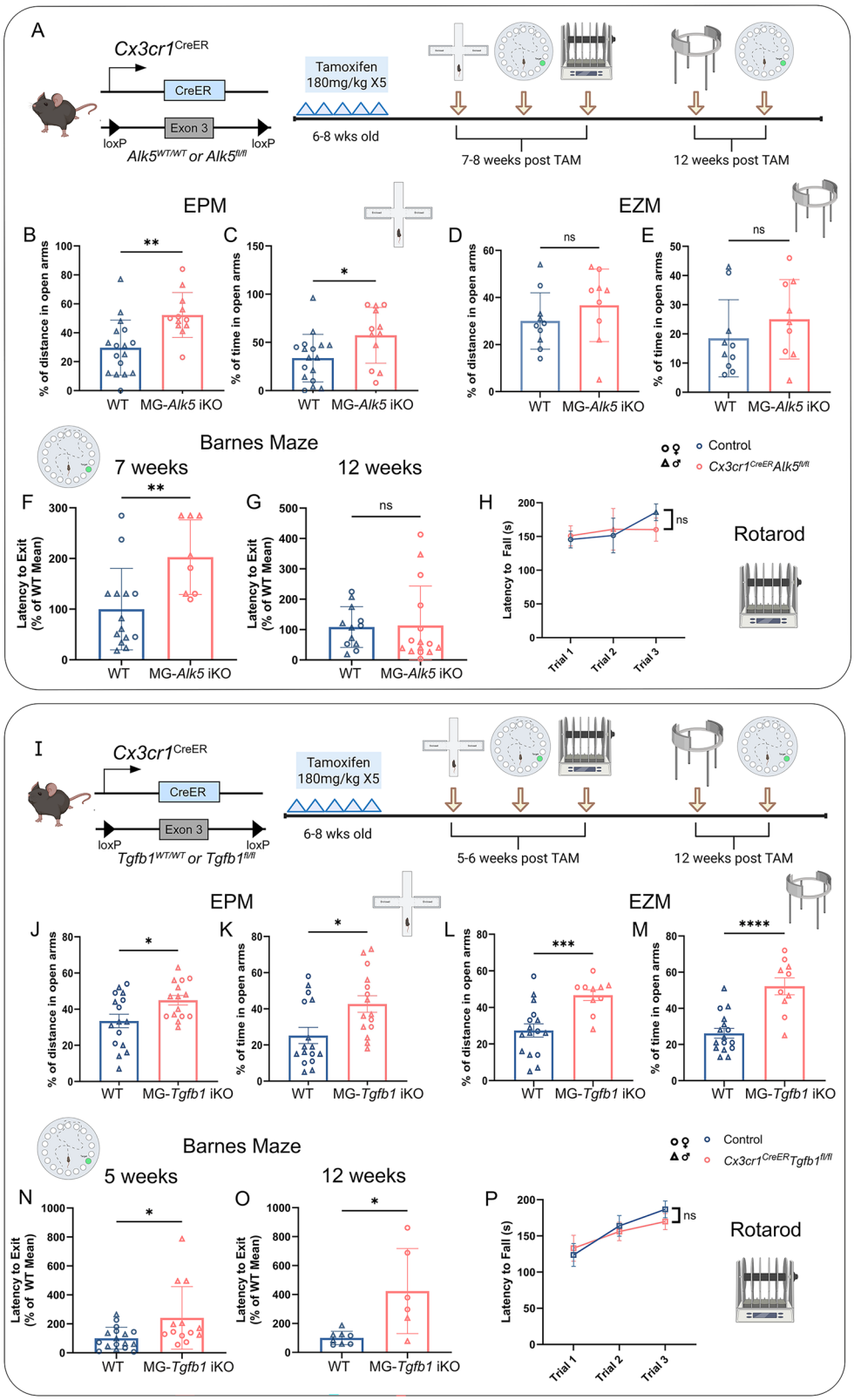

treatment. Importantly, this same phenotype is recapitulated in *Cx3cr1*^{CreER}-*Tgfb1*$^{fl/fl}$ ligand and *Cx3cr1*^{CreER}-*Tgfbr2*$^{fl/fl}$ type 2 receptor iKO, as well *P2ry12*$^{CreER/CreER}$-*Alk5*$^{fl/fl}$ iKO mice, all supporting that a TGF-β-deficient microglia profile is sufficient to drive enhanced adult neurogenesis. One potential caveat of the *P2ry12*^{CreER} driver is that previous studies[51,58] and our results both show that choroid plexus (ChP) macrophages could be targeted in this Cre line. The potential contribution of ChP macrophages in the iKO mouse lines cannot be completely ruled out and should be further investigated if new microglia-specific Cre driver lines are developed in the future. We propose a model of feedback regulation based on microglia or choroid plexus macrophages sensing neuronal damage (via DAMPs released by dying or injured neurons), which activates microglia/ ChP macrophages and subsequently stimulates neurogenesis as a compensatory mechanism

Fig. 10 | Silencing microglial TGF-β signaling results in altered behavior in cognitive and affective functional tests. A Mouse model used to induce *Alk5* KO in microglia and the experimental timeline depicts behavioral measurements at early and late time points after tamoxifen. **B**–**G** Behavioral measurements in *Cx3cr1*^{CreER}-*Alk5*$^{WT/WT}$ or *Cx3Cr1*^{CreER}-*Alk5*$^{fl/fl}$ mice showing elevated plus maze (**B**, **C**) at 7 weeks or elevated zero maze (**D**, **E**) at 12 weeks after TAM with percentage of distance in open arms, or percentage of time spent in open arms.**F**, **G** Barnes maze test at 7 weeks or 12 weeks post TAM. **H** Accelerated rotarod learning test. **B**, **C** WT $n = 17$, iKO $n = 12$; (**D**, **E**) WT $n = 10$, iKO $n = 9$; **F** WT $n = 17$, iKO $n = 13$; **G** WT $n = 8$, iKO $n = 6$; **H** WT $n = 8$, iKO $n = 8$. (** $p = 0.0022$ **B**, * $p = 0.0249$ **C**, ns=not significant (**D**, **E**, **G**, **H**), ** $p = 0.0079$ **F**). **I** Mouse model (left) used to induce *Tgfb1* KO in microglia and the experimental timeline depicts behavioral measurements at early or late time points after tamoxifen. **J**–**O** Behavioral measurements in *Cx3cr1*^{CreER}-*Tgfb1*$^{WT/WT}$ or *Cx3Cr1*^{CreER}- *Tgfb1*$^{fl/fl}$ mice showing elevated plus maze (**J**, **K**) at 6 weeks or elevated zero maze (**L**, **M**) at 12 weeks after TAM with percentage of distance in open arms, or percentage of time spent in open arms. **N**, **O** Barnes maze test at 6 weeks or 12 weeks post TAM. **P** Accelerated rotarod learning test[36]. **J**, **K** WT $n = 16$, iKO $n = 15$; (**L**, **M**) WT $n = 16$, iKO $n = 10$; **N** WT $n = 17$, iKO $n = 13$; **O** WT $n = 8$, iKO $n = 6$; **P** WT $n = 19$, iKO $n = 13$. (* $p = 0.0195$ **J**, * $p = 0.0111$ **K**, *** $p = 0.0004$ **L**, **** $p = 0.0002$ **M**, * $p = 0.0408$ **N**, * $p = 0.0428$ **O**, ns=not significant **P**). Two-sided Student's t-test analysis was used for statistical analysis in panels **B**–**G**, **J**–**O** and Two-way ANOVA RM, two-sided, with Tukey's post hoc pairwise analysis was used for statistical analysis in panels (**H**,**P**). Mean ± SE. The sex of each animal is represented by open circles (females) and open triangles (males). Panel **A** and **I** were created Created in BioRender. Luo, A. (2026) https://BioRender.com/6r2py3z. Source data are provided as a source data file.

to repair the injured CNS. Interestingly, some previous studies also support this proposed model. It was reported that SVZ microglia adopt a distinct profile resembling reactive microglia, and inhibition of this inflammatory-like profile by minocycline treatment leads to reduced SVZ neurogenesis[66]. This model also aligns well with the observation that CNS injuries that stimulate neurogenesis are also accompanied by neuroinflammation, such as in the case of stroke or TBI[15,22,23]. Our data reveals a comprehensive and complex role neuroinflammation could have in neurorepair, further cautioning the utilization of pan-immunosuppressant strategies to treat CNS injury[87,88]. The profile in MG-*Alk5* iKO microglia at 3 weeks of gene deletion might represent a pro-neurogenic microglia profile, which warrants further investigation in future studies.

We also explored the potential cell-cell interactions and mechanisms between the TGF-β signaling-silenced iKO microglia and the adult neurogenic cascade. Our data suggest a mechanism of enhanced survival of newly born neuroblasts in the iKO mice. Indeed, only 30% of the newly born cells in the adult SGZ survive to mature neurons, a very selective process the purpose of which is still not clear[89] which is consistent with the survival rate of BrdU+ cells in the SGZ in our control mice from 3wk-12wk post TAM while survival rate of BrdU/NeuN+ cells is increased to ~50% in the iKO mice. Nevertheless, while strategies to enhance the proliferation of adult NSCs might have caveats of potential safety issues with cancer risk, strategies to boost the survival of newly born cells in the SGZ has shown to be effective at increasing adult born neurons at the SGZ, for example by gene deletion of BAX, the pro-apoptotic factor in adult NSCs using *Nestin*^{CreER} driver in the iBAX mice. iBAX mice show enhanced SGZ adult neurogenesis and reduced anxiety and depression related behaviors in mice[17,90]. Interestingly, MG-*Alk5* iKO and MG-*Tgfb1* iKO mice both show increased SGZ neurogenesis and increased time/distance in the open arm in the elevated plus maze, a behavioral test considered a classic anxiety-related test. Importantly, since *MG-Alk5* iKO mice and *MG-Tgfb1* iKO show different temporal profiles in the microglia phenotype, with *Alk5* iKO recovering at 12 weeks and *Tgfb1* iKO remaining reactive at 12 weeks after TAM treatment, this difference allowed us to investigate whether the behavioral phenotype is consistent with the microglia phenotype. Indeed, our data show that both phenotypes in neurogenesis and behavioral outcome in the elevated mazes align well with the microglia phenotype in the two mouse models. In addition, our previous study using NSC-specific sonic hedgehog silencing in mice[45] showed decreased SGZ neurogenesis and decreased time/distance in the open arm in the EPM, supporting that adult neurogenesis could play an important role in this behavior. The mechanism by which *Alk5* iKO microglia recover but *Tgfb1* iKO microglia persist in reactivity at least up to 12 weeks is not known and warrants further investigation in future studies.

Several important homeostatic signature genes have been implicated in regulating SGZ neurogenesis, such as P2RY12[35] and CX3CR1[56] receptors. However, they are unlikely to be the mediator for enhanced neurogenesis in our model system. MG-*Alk5* and MG-*Tgfb1* iKO microglia both downregulate *P2ry12* and *Cx3cr1* expression, but previous studies have reported that *P2ry12* and *Cx3cr1* KO mice show reduced neurogenesis. ScRNAseq analysis identifies multiple ligand-receptor pairs that could mediate strong microglia-endothelial and microglia-DCX+ cell interactions, including multiple TGF-β mediated signaling pathways (Fig. 7). We chose to focus on cellular processes and pathways that are directly altered in immature neurons. These pathways include IGF-1, TNF-α, and PTEN-PI3K/mTOR pathways. It has been reported that reactive microglia releases IGF-1 and promotes adult neurogenesis in vitro[41]. More recently, Mir et al. showed that IGF-1 mediates neurogenesis via Sox2 activation in an Akt-dependent manner[40]. Given that our data show increased *Igf1* expression in iKO microglia and upregulated IGF-1 signaling in neuroblasts derived from iKO mice, we hypothesized that IGF-1 secreted from TGF-β-deficient microglia might be the mechanism of enhanced SGZ adult neurogenesis. Using *Alk5/Igf1* double iKO, we show successful gene deletion of *Alk5* and *Igf1* in dKO microglia; however, this does not reverse the phenotype of enhanced neurogenesis. While peripheral IGF-1 delivery[40,62] and overexpression of IGF-1 in mice[91] promote neurogenesis, these methods could result in systemic effects that are not restricted to the CNS. It is also possible that other cell types could upregulate *Igf1* which will not be abolished by MG-*Igf1* iKO. Future studies could further interrogate this scenario by utilizing NSC-specific (*Nestin*^{CreER})- or Neuroblast-specific DCX-specific (*DCX*^{CreER}) -*Igf1r* receptor KO mice. Alternatively, there might be a species difference between humans and mice. A recent study shows that human microglia-derived IGF-1 is critical for the regulation of neuroblasts in the human medial ganglionic eminence, while mouse *MG-Igf1* iKO does not show a similar effect[92]. Additionally, our results also show that *Tnf* KO does not rescue the phenotype of increased neurogenesis in our mouse model, suggesting that TNF-α is not required for the observed phenotype in our mouse model. However, there are many other growth factors and neurotrophic factors that have been reported to play an important role in regulating adult neurogenesis, such as brain-derived neurotrophic factor (BDNF)[93], Fibroblast Growth Factor (FGF)[14], Nerve Growth Factor (NGF), and Vascular Endothelial Growth Factor (VEGF)[94]. These factors may act synergistically in combination with other regulatory mechanisms to mediate adult hippocampal neurogenesis, a possibility that warrants further exploration in future studies using combinatory blockage or inhibition of downstream convergent signaling pathways.

The increase in DCX+ cells in *Cx3cr1*^{CreER}-*Alk5*$^{fl/fl}$ mice likely results from enhanced survival rather than increased proliferation. BrdU labeling three weeks post-TAM showed a sustained increase in BrdU+ cells up to 12 weeks. However, post-labeling these cells after TAM does not allow us to determine if this increased population of DCX+ cells is due to increased proliferation or increased survival. To circumvent this caveat, we showed that pre-labeling cells with BrdU before TAM treatment reflected an increase in the presence of BrdU+ cells 3 weeks

post-TAM, suggesting that the deletion of *Alk5* in microglia enhances the survival of adult-born neurons in the hippocampus. This is consistent with the absence of altered proliferation in the *Cx3cr1*^{CreER}-*Alk5*$^{fl/fl}$ mice and highlights the potential role of microglia beyond their traditional functions in phagocytosis or synaptic pruning, suggesting they may also play a key role in regulating neuronal survival in the hippocampus. Additionally, microglia ablation does not alter neurogenesis in *Nestin*^{CreER}-*tdTomato* mice, suggesting this enhanced survival in the MG-*Alk5* iKO mice is not merely due to the loss of an inhibitory role of microglia on adult neurogenesis.

The mammalian target of rapamycin (mTOR) signaling pathway, particularly through PTEN, plays a significant role in the survival of adult-born neurons[95]. Our scRNAseq analysis from *Cx3cr1*^{CreER}-*Alk5*$^{fl/fl}$ mice indicates reduced PTEN expression and increased PI3K/mTOR pathway in newly born neuroblasts, supporting our hypothesis that enhanced survival contributes to increased DCX+ at 3 weeks and BudU + /NeuN+ new neurons at 6- and 12 weeks after TAM. Here, we demonstrate that rapamycin treatment in MG-*Alk5* iKO mice, administered post-TAM treatment, reverses increased adult neurogenesis, further supporting a survival mechanism through the mTOR pathway. Loss of function of PTEN and upregulation of mTOR have been implicated in epilepsy (the top disease-related pathway identified in both MG-*Alk5* and MG-*Tgfb1* iKO mice in our study), known to be a classic model of aberrantly enhanced adult SGZ neurogenesis in which rapamycin treatment could also diminish the elevated neurogenesis and mossy fiber sprouting[96,97]. Interestingly, rapamycin has also been shown to be able to reverse TBI-induced SGZ neurogenesis[98], supporting that upregulation of mTOR pathway in the SGZ mediated by reactive microglia could be a common mechanism for other CNS-injury induced neurogenesis increase as well. Since OPCs are also moderately increased in our iKO mice, to test whether microglia directly interact with differentiating neuroblasts, using 3D primary NSC-microglia coculture, our data show that *Alk5* KO microglia directly increase neuronal differentiation in adult NSCs, which is also rescued by rapamycin treatment. These data support direct microglia-NSCs crosstalk via the mTOR mechanism. Importantly, our data show that the *Alk5* iKO microglia treated with rapamycin shows a similar activation index compared to iKO microglia treated with a vehicle, supporting that the reverse of phenotype in SGZ neurogenesis is not mediated through inhibition of microglia activation. In addition to the PTEN-mTOR axis, our data also show changes in PTEN-dependent cell cycle arrest and apoptosis, which could be a potential mechanism underlying the increased survival of immature neuroblasts in vivo. Additionally, GO enrichment analysis from the overlapping DEGs from both *Alk5* and *Tgfb1* iKO hippocampus shows upregulation of genes or other converging pathways (such as sonic hedgehog signaling[99] associated with GO terms including neurogenesis (GO:0022008), synaptic organization (GO:0050808), neuron projection development (GO:0031175), neuronal differentiation (GO:0030182) and neuron projection morphogenesis (GO:0048812). Some potentially interesting genes include Semaphorin-6B (*Sema6b*), with proposed functions in neuronal migration, axonal guidance, and hippocampal development[100,101], and Zinc finger MYND domain-containing protein 11 (*ZMYND11*), a gene whose function has recently been discovered to be critical for neurogenesis in humans[102]. In conclusion, our study highlights the critical role of microglia-derived TGF-β signaling in regulating microglia profile and, in turn, regulating adult neurogenesis, particularly in neuronal survival and integration into the neural circuitry. Targeting TGF-β signaling in microglia or targeted modulation of microglia profile may offer potential therapeutic strategies to enhance neurogenesis in aging or in neurodegenerative conditions.

This study bridges the gap in our understanding of the direct causal role of microglia on regulating SGZ adult neurogenesis and the molecular pathways mediating the crosstalk between these two critical cellular processes, shedding light on potential therapeutic strategies for enhancing neuroplasticity under physiological and neurodegenerative conditions.

Limitations of our study include a lack of brain regional manipulation of microglia TGF-β signaling, which is a technical limitation of the current field. Additionally, we do not show direct functional contributions of the elevated adult neurogenesis to the observed behavioral alterations in EPM. This is difficult to achieve with the combination of microglia-specific gene manipulation. Two alternative methods have been traditionally used to target NSC cells, which may help establish the direct causal contribution of the increased neurogenesis to the functional outcome in our mouse models. One of them is to deliver anti-mitotic agents intracerebrally to transiently inhibit neurogenesis at SVZ or SGZ. This method will introduce a confound in our study as iKO microglia are also proliferating and could potentially be affected by this intervention directly. Another potential method is to use retroviral-delivered inhibitory Designer Receptors Exclusively Activated by Designer Drugs (DREADDs) to inhibit the function of adult-born neurons; however, injecting the virus into the hippocampus can trigger microglial reactivity, which introduces a confound in studies of microglia-NSCs crosstalk. Alternatively, if FLP-FRT (Flippase-Flp Recombination Target sites) models were available for adult NSC lineage, induced expression of excitatory or inhibitory ion channels can be achieved in NSCs on an MG-*Alk5* iKO background, which could allow investigation of the direct contribution of elevated neurogenesis to the behavioral outcome. In addition, the Barnes maze was used to evaluate general learning/memory functions in the *Alk5* and *Tgfb1* iKO mice in our previous[36] and this study; however, reverse learning was not achieved in our study, likely due to the mild aversive cues we used in our test setting. Previous studies have demonstrated that reverse learning in tasks such as the Morris Water Maze is sensitive to the status of neurogenesis in adult mice[103,104], which could be included in future studies. Finally, we included both sexes in our study and annotated the sex of each animal in all figures. We did not observe an overall difference in the microglia phenotype or neurogenesis phenotype in our experiments; however, our study was not powered or intended to detect sex differences.

Methods

Animals

Laboratory Animal Medical Services (LAMS), Animal Care and Use Program (ACUP) and the Institutional Animal Care and Use Committee (IACUC) are housed at the University of Cincinnati. All animal protocols were approved by IACUC. Approved animal protocol number is 24-02-27-01. Within LAMS, mice are held to a 14 h light/10 h dark cycle. *Nestin*^{CreER} (JAX:016261)[59] and Ai9 *R26-CAG-tdTomato* (JAX:007909)[105] were used to endogenously label and track NSCs. We generated cell-type-specific inducible knockout models of critical TGF-β signaling components using *Cx3cr1*$^{CreER(Jung)}$ (JAX:020940)[53], *Cx3cr1*$^{CreER(Littman)}$ (JAX:021160)[54], and *P2ry12*^{CreER} (JAX:034727)[58], to delete *Alk5*, *Tgfbr2*, *Igf1* in microglia or *Tnfα* constitutive knockout. *Alk5* (JAX:028701)[106] floxed or *Tgfbr2* (JAX:012603)[107] floxed mice, and *Tnfα* KO (JAX:005540)[108] and *Igf1* floxed (JAX:016831)[109] mice were crossed with *Cx3cr1*$^{CreER(Jung)}$, all purchased from the Jackson Laboratory. We crossed the above microglia *Cre*^{ER} lines with *ROSA26-YFP* (JAX:006148)[110] in some of the experiments to facilitate microglia sorting. All animals were euthanized by administration of avertin (2.5%) followed by transcardial perfusion with 4% paraformaldehyde (PFA) (for IHC) or 1x HBSS (for FACS, RNAseq, and qRT-PCR) as previously described[36]. Mice were bred on a C57BL/6 J background and both sexes were used in all experiments. All animals were used unless tissue quality was poor as a result of subpar perfusions or inadequate cryoprotection. For all experiments, bromodeoxyuridine (BrdU) was administered intraperitoneally at 100 mg/kg per injection (10 μl/g bodyweight, Invitrogen #000103) during the indicated time frame in each experimental timeline and harvested between 3-12 weeks post-TAM.

Tamoxifen administration

3 or 5 consecutive gavage injections of TAM (specified in each experiment/figure) solution were given to 6-16-week-old male and female mice, administered at a dosage of 180 mg/kg. 900 μL of sunflower seed oil and 100 μL of ethanol were sonicated with 30 mg of TAM powder protected from light[36]. To evaluate the effect of microglia-mediated TGF-β signaling silencing in adult neurogenesis, young adult mice were harvested at 3, 6-, or 12-weeks post-TAM to evaluate microglia phenotype and SGZ neurogenesis.

Microglia ablation PLX5622

Mice were given either the control diet (Plexxikon) or PLX5622 diet (Plexxikon) as previously described[36,111] for the duration of the study. All animals had unrestricted access to diet and water. For studying the phenotype of homeostatic microglia on baseline adult neurogenesis, we administered TAM to *Nestin*^{CreER}*-Ai9* mice to label aNSCs and their progeny, followed by 3 weeks of control or PLX5622 diet. Mice were harvested 3 weeks post-TAM and brains were harvested for IHC staining. For assessing the role of repopulating *Alk5* KO microglia in the stimulation of adult neurogenesis, mice were treated with a control PLX5622 diet for 3 weeks, followed by TAM treatment during the last 3 days. These animals were then switched to a standard chow diet to allow the repopulation of WT or *Alk5* KO microglia over the course of 3 weeks, when they were harvested by administration of avertin (2.5%) followed by transcardial perfusion with 4% paraformaldehyde (PFA). Brain tissue was harvested for IHC staining.

Fluorescent activated cell sorting (FACS)

Mice were harvested by administration of avertin (2.5%) followed by transcardial perfusion with cold 1xHBSS for 3–4 mins before the brain was extracted. The brains were mechanically dissociated via a scalpel before enzymatically dissociated with the papain dissociation system (9001-73-4, Worthington Biochemical Corporation) while all of the above processes are carried out in the presence of transcriptional and translational inhibitors to prevent microglial gene expression changes during the isolation protocol[60]. Once the brain is sufficiently dissociated, 37% percoll solution was used to clear any excess myelin or debris. Cells were resuspended in FACS buffer (0.5% BSA in PBS) for staining and sorting using a BD/FACSAria II (BD Biosciences, Franklin Lakes, NJ). CD11b, CD45, and GFP reporter were used to develop a gating strategy to enrich microglia. Sorted microglial cells were used for qRT-PCR or bulk RNAseq for gene expression analysis as described below.

qRT-PCR

Using the RNAqueous- Micro Total RNA isolation kit (AM1931, Thermo Fisher Scientific), RNA was isolated from sorted microglia as previously described[36]. Supercript III reverse transcriptase (18080044, ThermoFisher Scientific) or iScript cDNA synthesis kit (1708890, BioRad) was used to generate cDNA. Following cDNA synthesis, qRT-PCR probes *Hmbs1* (hydroxymethylbilane synthase), *Hprt1* (hypoxanthine phosphoribosyltransferase 1), *Aif1, Alk5, Igf1, Tnf, Tmem119*, and *P2ry12* were used to analyze cDNA levels using a Roche Light Cycler II 480. Relative gene expression was calculated using the ΔΔCt method compared to Hmbs1 as a reference gene and expressed as fold change compared to the average of control cells for each individual gene.

Immunohistochemistry

Mice were anesthetized with avertin (2.5%), then perfused with 4% PFA. The brains were harvested and post-fixed in 4% PFA overnight. In the following days, brains were switched to 20% and 30% sucrose respectively until brains sank. Each brain was sectioned at 30 μM thickness on a cryostat and used for immunohistochemistry (IHC) staining as previously described[36]. Antibodies for BrdU (1:500, Abcam), DCX (1:1000, Cell Signaling), Ki67 (1:500, Invitrogen), IBA1 (1:1000, Abcam), TMEM119 (1:2000, GeneTex), P2RY12 (1:200, Biolegend), GFAP (1:1000, Sigma), pSMAD3 (1:200, Abcam), beta-3 tubulin (1:2000, Promega), pS6 (1:800, Cell Signaling), Olig2 (1:500, R&D Systems), MBP (1:250, Biorad), NG2 (1:500, Millipore) were used. P2RY12 clone: P2YM 17A12[112] (1:500), and P2RY12 clone: P2YM 1E5[112] (1:500) was generated and validated as previously described. Brain sections were blocked for 1 h at room temperature in 4% BSA/0.3% Triton-x100 and incubated in primary antibody solution (diluted in blocking buffer) on a shaker overnight at 4 °C. Secondary antibodies conjugated with Alexa fluorescence 488, 555, 647 or 790 (1:500) were incubated with the brain sections for 4 hours at room temperature. Confocal imaging of stained brain sections was carried out using a Leica Stellaris 8. Quantification of cell counts was carried out using ImageJ (1.53) software. At least 3 coronal sections with the respective region of interest were quantified for each mouse and averaged to be used as a single data point.

BrdU Immunohistochemistry

Animals injected with BrdU labeling reagent (10 μl/g bodyweight, Invitrogen #000103) at various time points after injection were harvested following avertin (2.5%) injection and PB/PFA perfusion. As described previously[113], coronal or sagittal cryosections were washed 3x at RT and incubated in pre-warmed freshly made DNA denaturation solution (50% formamide, 50% 2x SSC buffer) for 2 hours at 60 °C with shaking. After being washed 3x in 2x SSC at 60 °C with shaking, the tissue was incubated in 2 N HCl at 37 °C with shaking. Then, the sections were incubated 1x in borate buffer (pH 8.5) at RT with shaking for 10 min and washed 1x in PB at RT. The tissue was blocked in blocking buffer for 1 h at RT and the standard immunofluorescent protocol was followed (see Immunohistochemistry above).

scRNAseq

Single-cell RNA sequencing was performed at Single Cell Discoveries (https://www.scdiscoveries.com/) according to the 10x Genomics Single Cell Gene Expression Flex solution protocol. Mice were anesthetized with avertin (2.5%), then perfused with 1x PB before whole hippocampal pieces were micro-dissected from the brain and flash-frozen on dry ice. Samples were shipped on dry ice to Single Cell Discoveries where all Processing of samples was performed by Single Cell sequencing experts. For each sample, 8000–14,000 cells were loaded and sequencing libraries were prepared following a standard 10x Genomics protocol.

As similarly described by others[114], sample reads were aligned to the mouse genome GRCm39 (Datasets - 10x Genomics) using Cell Ranger 9.0.0 Flex pipeline (Flex with Cell Ranger multi - Official 10x Genomics Support). The data from all samples were loaded in R (version 4.3.2) and processed using the Seurat package (5.1.0). Cells expressing least 200 genes and less than 20% mitochondrial gene content were retained for analysis. The data of all 10x libraries was merged and processed together and normalized for sequencing depth per cell and log transformed. After data cleaning and filtering, datasets were integrated using Harmony[115]. Following this, clustering was done using the FindNeighbors function (dims=1:20) at a resolution of 0.12. To identify cell types in separate clusters, signature genes for each cell type were used based on the Cell Marker 2.0 database for mouse species in brain tissue. To analyze differentially expressed genes (DEGs) between control and MG-*Alk5* or MG-*Tgfb1* iKO samples, we used FindMarkers to filter for genes that were expressed in at least 10% of cells in either of the conditions and had an adjusted p-value of <0.05. DEGs from either neuroblast or microglia cluster were plotted onto a volcano plot using R packages DESeq2 and EnhancedVolcano. These DEGs were input into EnrichR for pathway enrichment analysis. Intercellular signaling was profiled using LIANA (v0.2.0). LIANA aggregated predictions from multiple computational methods (including CellPhoneDB, NATMI, SCA and LogFc) and ranked interactions based on the consensus mean rank score. The Mouse Consensus

ligand–receptor database was used as the reference resource. Visualization of significant ligand–receptor pairs was generated using ggplot2 based on LIANA's aggregated output.

Rapamycin treatment

To evaluate the contributions of mTOR signaling on adult neurogenesis after deletion of microglia-mediated ALK5 signaling, control or MG-*Alk5* iKO mice received TAM for 5 days to delete *Alk5* in microglia. Daily intraperitoneal (I.P.) injections of rapamycin were given starting from the 4th day of TAM for 21 days to 4-6-month-old male and female mice, administered at a dosage of 10 mg/kg similar to previous studies[96,98]. 5% PEG400 and 5% Tween80 was diluted into MQH2O with 4% rapamycin (diluted in EtOH) or 4% EtOH to generate a working solution of 1 mg/mL. Mice were harvested 3 weeks post-TAM by administering avertin (2.5%) and then transcardially perfused with 4% paraformaldehyde (PFA).

Tissue culture

Isolation of primary adult neural stem cells (aNSCs) from C57B6J WT mice is established as previously described[5]. Mice (6-week-old) were culled by cervical dislocation, and the SVZ was microdissected and dissociated into single cells. Adult NSCs are cultured with neurobasal media containing heparin, EGF, bFGF, and B-27 as described in our previous studies[5,116,117]. Single cells are cultured as neurospheres in the media above. Neurospheres between passages 5 and 7 were used for in vitro experiments where the disassociated single cells were plated at 3×10^3 cells/well in a ultra-low attachment 96-well round-bottom plate. These aNSCs were then given 5 days to form a sphere and proliferate before co-cultured with primary mouse microglia (mMG). The mMG used was obtained from P3 pups with a *P2ry12*$^{CreERT/CreERT2}$-*Alk5*$^{WT/WT}$ *or P2ry12*$^{CreERT2/CreERT2}$-*Alk5*$^{fl/fl}$ genotype via a mixed glial culture of the whole brain (excluding the olfactory bulb and cerebellum). The tissue collected and processed were put into a poly-D-lysine coated T75 flask with one flask per pup in glial media (DMEM/F-12, 10% FBS, 1% 100X L-Glutamate, 1% Pen/Strep). Feeds consisting of glial media were given every 3 days. On day 11, the flasks were given 1 µM 4-OH TAM diluted in ethanol. On day 14, the flasks were then fed with glial media and shaken on an orbital shaker at 180 rpm for 3 h to collect WT or KO mMG. *Alk5* mRNA decrease in the KO mMG was confirmed by qRT-PCR. The collected WT or KO mMG (3000 cells per sphere) was added to the NSC neutrospheres to establish the 3D co-culture. 3 days after the microglia were added to the neurospheres, the media were changed to differentiation media consisting of neurobasal media without growth factors but with microglia serum (from ScienCell's microglia medium) to help maintain the microglia while differentiating the aNSCs. Additionally, 100 nM rapamycin or vehicle (ethanol) was added to the differentiation media. The co-culture was then differentiated for 4 days before fixation via 4% PFA. The fixed co-culture spheres were then stained by permeabilizing them via 0.3% 100X Triton in DPBS for 10 minutes, blocked with blocking buffer (4% BSA/0.3% 100X Triton) for 1 hour, incubated in primary antibody solution (βIII-Tubulin [1:2000, Promega] and GFAP [1:1000, BioLegend]) for 4 days at 4 C, washed with DPBS 4x, incubated in secondary antibodies (Donkey anti-Mouse 647 [1:500, Jackson ImmunoResearch] and Donkey anti-rabbit 488+ [1:1000, Invitrogen]) and DAPI diluted in blocking buffer for 3 days at 4 C, and washed 4x for 5 mins each. Neurospheres were then imaged using a Leica Stellaris 8 confocal microscope and quantified in ImageJ for % area of immunoreactivity.

Behavioral tests

EPM/EZM. Elevated Plus Maze (EPM) or Elevated Zero Maze (EZM) was used to assess anxiety-like behavior in mice. The EPM or EZM is elevated ~60 cm off the floor. The EPM consists of a cross-shaped platform that is 5 cm wide and 30 cm long with two opposing arms containing dark walls that are 15 cm high. The EZM is an O-ring-shaped platform that is 60 cm in diameter with a 5 cm wide platform. Two sections of the O-shaped apparatus are enclosed by dark walls 15 cm high. Black-out curtains surround the testing area to help maintain a consistent lighting of 18 lux via LED strips[45]. Animals are habituated to the room for at least 20 minutes before testing. In between each animal, the apparatus is cleaned with warm water and 10% Conflikt (Decon Labs). Each animal is allowed to freely explore the apparatus for 5 minutes before being returned to their home cage. EPM is the first behavioral test, and for the second anxiety test, EZM is used to prevent repeated exposure to the same maze. Data was automatically scored using AnyMaze (Stoelting Company, Wood Dale, IL).

Barnes maze. To evaluate spatial learning and memory in mice, the Barnes Maze apparatus (Stoelting Company, Wood Dale, IL) was used as previously described[36]. Using a short and challenging paradigm, we trained the animals in two separate sessions 4 h apart where the animals were motivated to locate the escape hole during each session with light and a fan. Animals were tested the following day. In between each animal, the apparatus was cleaned with warm water followed by 20% ethanol and allowed to dry. Data was automatically scored using AnyMaze (Stoelting Company, Wood Dale, IL).

Rotarod. Motor coordination and motor learning were assessed in animals using the Roto-rod Series 8 apparatus (IITC Life Science Inc., Woodland Hills, CA) with an acceleration paradigm starting at 5rpm and reaching a maximum of 20rpm over 300 seconds. Once each animal reached the end of the 300 seconds or fell off the rotating rod, they were returned to their cages after 3 consecutive trials with rest in between. The Roto-rod apparatus was sanitized using 70% ethanol in between each animal.

Quantification and statistical analysis

All data were analyzed using SigmaPlot (12.0) for statistical significance. Results are expressed by mean ± SEM of the indicated number of experiments. Statistical analysis was performed using the two-sided Student's t-test, two-sided Welch's t-test, and two-sided one- or -two-way analysis of variance (ANOVA), as appropriate, with Tukey's post hoc tests. A p-value to or less than 0.05 was considered significant. When the data did not meet the assumptions of normality or equal variance, the corresponding nonparametric tests were used. The significance level was set at $\alpha = 0.05$. Number of animals used in each experiment plotted as single data point and are indicated in Figure legends. Graphs were made in GraphPad Prism (10.6.1) and portions of figures were created with BioRender.com. The notation for p-values was as follows: n.s – $p \geq 0.05$, * – $p < 0.05$, ** – $p < 0.01$, *** – $p < 0.001$, **** – $p < 0.0001$.

Reporting summary

Further information on research design is available in the Nature Portfolio Reporting Summary linked to this article.

Data availability

The scRNA-seq data generated in this study have been deposited in the BioProject database under accession code BioProject: PRJNA1237411 (http://www.ncbi.nlm.nih.gov/bioproject/1237411). The rest of the data generated in this study are provided in the Supplementary Information/Source Data file. Any requests for information, reagents, and other resources should be directed to and will be fulfilled by the lead contact, Yu Luo (luoy2@ucmail.uc.edu). Source data are provided with this paper.

References

1. Ming, G. & Song, H. Adult Neurogenesis in the Mammalian Brain: Significant Answers and Significant Questions. *Neuron* **70**, 687–702 (2011).

2. Lledo, P.-M. & Valley, M. Adult Olfactory Bulb Neurogenesis. *Cold Spring Harb. Perspect. Biol.* **8**, a018945 (2016).
3. Moreno, M. M. et al. Olfactory perceptual learning requires adult neurogenesis. *Proc. Natl. Acad. Sci. Usa.* **106**, 17980–17985 (2009).
4. Arvidsson, A., Collin, T., Kirik, D., Kokaia, Z. & Lindvall, O. Neuronal replacement from endogenous precursors in the adult brain after stroke. *Nat. Med* **8**, 963–970 (2002).
5. Luo, F. et al. Inhibition of CSPG receptor PTPσ promotes migration of newly born neuroblasts, axonal sprouting, and recovery from stroke. *Cell Rep.* **40**, 111137 (2022).
6. Nath, S. et al. Interaction between subventricular zone microglia and neural stem cells impacts the neurogenic response in a mouse model of cortical ischemic stroke. *Nat. Commun.* **15**, 9095 (2024).
7. Jessberger, S. et al. Dentate gyrus-specific knockdown of adult neurogenesis impairs spatial and object recognition memory in adult rats. *Learn Mem.* **16**, 147–154 (2009).
8. Akers, K. G. et al. Hippocampal neurogenesis regulates forgetting during adulthood and infancy. *Science* **344**, 598–602 (2014).
9. Wang, C. et al. Microglia mediate forgetting via complement-dependent synaptic elimination. *Science* **367**, 688–694 (2020).
10. Anacker, C. & Hen, R. Adult hippocampal neurogenesis and cognitive flexibility — linking memory and mood. *Nat. Rev. Neurosci.* **18**, 335–346 (2017).
11. Frechou, M. A. et al. Adult neurogenesis improves spatial information encoding in the mouse hippocampus. *Nat. Commun.* **15**, 6410 (2024).
12. Van Praag, H., Kempermann, G. & Gage, F. H. Running increases cell proliferation and neurogenesis in the adult mouse dentate gyrus. *Nat. Neurosci.* **2**, 266–270 (1999).
13. Li, Z. et al. Enriched Environment Reduces Seizure Susceptibility via Entorhinal Cortex Circuit Augmented Adult Neurogenesis. *Adv. Sci.* **11**, 2410927 (2024).
14. Grońska-Pęski, M., Gonçalves, J. T. & Hébert, J. M. Enriched Environment Promotes Adult Hippocampal Neurogenesis through FGFRs. *J. Neurosci.* **41**, 2899–2910 (2021).
15. Cho, K.-O. et al. Aberrant hippocampal neurogenesis contributes to epilepsy and associated cognitive decline. *Nat. Commun.* **6**, 6606 (2015).
16. Liang, H. et al. Region-specific and activity-dependent regulation of SVZ neurogenesis and recovery after stroke. *Proc. Natl. Acad. Sci. Usa.* **116**, 13621–13630 (2019).
17. Hill, A. S., Sahay, A. & Hen, R. Increasing Adult Hippocampal Neurogenesis is Sufficient to Reduce Anxiety and Depression-Like Behaviors. *Neuropsychopharmacol* **40**, 2368–2378 (2015).
18. Ekdahl, C. T., Claasen, J.-H., Bonde, S., Kokaia, Z. & Lindvall, O. Inflammation is detrimental for neurogenesis in adult brain. *Proc. Natl. Acad. Sci. Usa.* **100**, 13632–13637 (2003).
19. Bassani, T. B. et al. Decrease in Adult Neurogenesis and Neuroinflammation Are Involved in Spatial Memory Impairment in the Streptozotocin-Induced Model of Sporadic Alzheimer's Disease in Rats. *Mol. Neurobiol.* https://doi.org/10.1007/s12035-017-0645-9 (2017).
20. Wu, M. D. et al. Adult murine hippocampal neurogenesis is inhibited by sustained IL-1β and not rescued by voluntary running. *Brain, Behav., Immun.* **26**, 292–300 (2012).
21. Chesnokova, V., Pechnick, R. N. & Wawrowsky, K. Chronic peripheral inflammation, hippocampal neurogenesis, and behavior. *Brain, Behav., Immun.* **58**, 1–8 (2016).
22. Jin, K. et al. Evidence for stroke-induced neurogenesis in the human brain. *Proc. Natl. Acad. Sci. Usa.* **103**, 13198–13202 (2006).
23. Willis, E. F. et al. Repopulating Microglia Promote Brain Repair in an IL-6-Dependent Manner. *Cell* **180**, 833–846.e16 (2020).
24. Ribeiro Xavier, A. L., Kress, B. T., Goldman, S. A., Lacerda De Menezes, J. R. & Nedergaard, M. A Distinct Population of Microglia Supports Adult Neurogenesis in the Subventricular Zone. *J. Neurosci.* **35**, 11848–11861 (2015).
25. Wallace, J., Lord, J., Dissing-Olesen, L., Stevens, B. & Murthy, V. N. Microglial depletion disrupts normal functional development of adult-born neurons in the olfactory bulb. *eLife* **9**, e50531 (2020).
26. Kyle, J., Wu, M., Gourzi, S. & Tsirka, S. E. Proliferation and Differentiation in the Adult Subventricular Zone Are Not Affected by CSF1R Inhibition. *Front. Cell. Neurosci.* **13**, 97 (2019).
27. Cserép, C. et al. Microglial control of neuronal development via somatic purinergic junctions. *Cell Rep.* **40**, 111369 (2022).
28. Diaz-Aparicio, I. et al. Microglia Actively Remodel Adult Hippocampal Neurogenesis through the Phagocytosis Secretome. *J. Neurosci.* **40**, 1453–1482 (2020).
29. Sierra, A. et al. Microglia Shape Adult Hippocampal Neurogenesis through Apoptosis-Coupled Phagocytosis. *Cell Stem Cell* **7**, 483–495 (2010).
30. Nakaso, K. Roles of Microglia in Neurodegenerative Diseases. *Yonago Acta Med* **67**, 1–8 (2024).
31. Antignano, I., Liu, Y., Offermann, N. & Capasso, M. Aging microglia. *Cell. Mol. Life Sci.* **80**, 126 (2023).
32. Badanjak, K., Fixemer, S., Smajić, S., Skupin, A. & Grünewald, A. The Contribution of Microglia to Neuroinflammation in Parkinson's Disease. *IJMS* **22**, 4676 (2021).
33. Deczkowska, A. et al. Disease-Associated Microglia: A Universal Immune Sensor of Neurodegeneration. *Cell* **173**, 1073–1081 (2018).
34. Araki, T., Ikegaya, Y. & Koyama, R. The effects of microglia- and astrocyte-derived factors on neurogenesis in health and disease. *Eur. J. Neurosci.* **54**, 5880–5901 (2021).
35. Mo, M. et al. Microglial P2Y12 Receptor Regulates Seizure-Induced Neurogenesis and Immature Neuronal Projections. *J. Neurosci.* **39**, 9453–9464 (2019).
36. Bedolla, A. et al. Adult microglial TGFβ1 is required for microglia homeostasis via an autocrine mechanism to maintain cognitive function in mice. *Nat. Commun.* **15**, 5306 (2024).
37. Butovsky, O. et al. Identification of a unique TGF-β–dependent molecular and functional signature in microglia. *Nat. Neurosci.* **17**, 131–143 (2014).
38. Zöller, T. et al. Silencing of TGFβ signalling in microglia results in impaired homeostasis. *Nat. Commun.* **9**, 4011 (2018).
39. Arjunan, A., Sah, D. K., Woo, M. & Song, J. Identification of the molecular mechanism of insulin-like growth factor-1 (IGF-1): a promising therapeutic target for neurodegenerative diseases associated with metabolic syndrome. *Cell Biosci.* **13**, 16 (2023).
40. Mir, S., Cai, W., Carlson, S. W., Saatman, K. E. & Andres, D. A. IGF-1 mediated Neurogenesis Involves a Novel RIT1/Akt/Sox2 Cascade. *Sci. Rep.* **7**, 3283 (2017).
41. Butovsky, O. et al. Microglia activated by IL-4 or IFN-γ differentially induce neurogenesis and oligodendrogenesis from adult stem/progenitor cells. *Mol. Cell. Neurosci.* **31**, 149–160 (2006).
42. Buttgereit, A. et al. Sall1 is a transcriptional regulator defining microglia identity and function. *Nat. Immunol.* **17**, 1397–1406 (2016).
43. Navabi, S. P. et al. Microglia-induced neuroinflammation in hippocampal neurogenesis following traumatic brain injury. *Heliyon* **10**, e35869 (2024).
44. Rahman, A. A., Amruta, N., Pinteaux, E. & Bix, G. J. Neurogenesis After Stroke: A Therapeutic Perspective. *Transl. Stroke Res.* **12**, 1–14 (2021).
45. Wang, J. et al. Disruption of Sonic Hedgehog signaling accelerates age-related neurogenesis decline and abolishes stroke-induced neurogenesis and lead to increased anxiety behavior in stroke mice. *Transl. Stroke Res* **13**, 830–844 (2022).

46. Jin, K. Neurogenesis in the aging brain. *CIA* **2**, 605–610 (2008). **Volume**.
47. Ryu, J. R. et al. Control of adult neurogenesis by programmed cell death in the mammalian brain. *Mol. Brain* **9**, 43 (2016).
48. Hata, A. & Chen, Y.-G. TGF-β Signaling from Receptors to Smads. *Cold Spring Harb. Perspect. Biol.* **8**, a022061 (2016).
49. Goebel, E. J. et al. Structural characterization of an activin class ternary receptor complex reveals a third paradigm for receptor specificity. *Proc. Natl. Acad. Sci.* **116**, 15505–15513 (2019).
50. Bedinger, D. et al. Development and characterization of human monoclonal antibodies that neutralize multiple TGFβ isoforms. *mAbs* **8**, 389–404 (2016).
51. Bedolla, A. M. et al. A comparative evaluation of the strengths and potential caveats of the microglial inducible CreER mouse models. *Cell Rep.* **43**, 113660 (2024).
52. Faust, T. E. et al. A comparative analysis of microglial inducible Cre lines. *Cell Rep.* **42**, 113031 (2023).
53. Yona, S. et al. Fate Mapping Reveals Origins and Dynamics of Monocytes and Tissue Macrophages under Homeostasis. *Immunity* **38**, 79–91 (2013).
54. Parkhurst, C. N. et al. Microglia Promote Learning-Dependent Synapse Formation through Brain-Derived Neurotrophic Factor. *Cell* **155**, 1596–1609 (2013).
55. Reshef, R. et al. The role of microglia and their CX3CR1 signaling in adult neurogenesis in the olfactory bulb. *eLife* **6**, e30809 (2017).
56. Rogers, J. T. et al. CX3CR1 Deficiency Leads to Impairment of Hippocampal Cognitive Function and Synaptic Plasticity. *J. Neurosci.* **31**, 16241–16250 (2011).
57. Bachstetter, A. D. et al. Fractalkine and CX3CR1 regulate hippocampal neurogenesis in adult and aged rats. *Neurobiol. Aging* **32**, 2030–2044 (2011).
58. McKinsey, G. L. et al. A new genetic strategy for targeting microglia in development and disease. *eLife* **9**, e54590 (2020).
59. Lagace, D. C. et al. Dynamic Contribution of Nestin-Expressing Stem Cells to Adult Neurogenesis. *J. Neurosci.* **27**, 12623–12629 (2007).
60. Marsh, S. E. et al. Dissection of artifactual and confounding glial signatures by single-cell sequencing of mouse and human brain. *Nat. Neurosci.* **25**, 306–316 (2022).
61. Nieto-Estévez, V., Defterali, Ç. & Vicario-Abejón, C. IGF-I: A Key Growth Factor that Regulates Neurogenesis and Synaptogenesis from Embryonic to Adult Stages of the Brain. *Front. Neurosci.* **10**, (2016).
62. Åberg, M. A. I., Åberg, N. D., Hedbäcker, H., Oscarsson, J. & Eriksson, P. S. Peripheral Infusion of IGF-I Selectively Induces Neurogenesis in the Adult Rat Hippocampus. *J. Neurosci.* **20**, 2896–2903 (2000).
63. Zeger, M. et al. Insulin-like growth factor type 1 receptor signaling in the cells of oligodendrocyte lineage is required for normal in vivo oligodendrocyte development and myelination. *Glia* **55**, 400–411 (2007).
64. Nakajima, S., Ohsawa, I., Ohta, S., Ohno, M. & Mikami, T. Regular voluntary exercise cures stress-induced impairment of cognitive function and cell proliferation accompanied by increases in cerebral IGF-1 and GST activity in mice. *Behavioural Brain Res.* **211**, 178–184 (2010).
65. Chen, Z. & Palmer, T. D. Differential roles of TNFR1 and TNFR2 signaling in adult hippocampal neurogenesis. *Brain, Behav., Immun.* **30**, 45–53 (2013).
66. Shigemoto-Mogami, Y., Hoshikawa, K., Goldman, J. E., Sekino, Y. & Sato, K. Microglia Enhance Neurogenesis and Oligodendrogenesis in the Early Postnatal Subventricular Zone. *J. Neurosci.* **34**, 2231–2243 (2014).
67. Yonan, J. M., Chen, K. D., Baram, T. Z. & Steward, O. PTEN deletion in the adult dentate gyrus induces epilepsy. *Neurobiol. Dis.* **203**, 106736 (2024).
68. Forner, S. et al. Systematic phenotyping and characterization of the 5xFAD mouse model of Alzheimer's disease. *Sci. Data* **8**, 270 (2021).
69. Stazi, M. & Wirths, O. Chronic Memantine Treatment Ameliorates Behavioral Deficits, Neuron Loss, and Impaired Neurogenesis in a Model of Alzheimer's Disease. *Mol. Neurobiol.* **58**, 204–216 (2021).
70. Ge, S., Yang, C., Hsu, K., Ming, G. & Song, H. A critical period for enhanced synaptic plasticity in newly generated neurons of the adult brain. *Neuron* **54**, 559–566 (2007).
71. Rodgers, R. J. & Shepherd, J. K. Influence of prior maze experience on behaviour and response to diazepam in the elevated plus-maze and light/dark tests of anxiety in mice. *Psychopharmacol. (Berl.)* **113**, 237–242 (1993).
72. File, S. E., Mabbutt, P. S. & Hitchcott, P. K. Characterisation of the phenomenon of 'one-trial tolerance' to the anxiolytic effect of chlordiazepoxide in the elevated plus-maze. *Psychopharmacol. (Berl.)* **102**, 98–101 (1990).
73. Alonso, M., Petit, A.-C. & Lledo, P.-M. The impact of adult neurogenesis on affective functions: of mice and men. *Mol. Psychiatry* **29**, 2527–2542 (2024).
74. Sahay, A. et al. Increasing adult hippocampal neurogenesis is sufficient to improve pattern separation. *Nature* **472**, 466–470 (2011).
75. Gonçalves, J. T., Schafer, S. T. & Gage, F. H. Adult Neurogenesis in the Hippocampus: From Stem Cells to Behavior. *Cell* **167**, 897–914 (2016).
76. Kempermann, G. What Is Adult Hippocampal Neurogenesis Good for?. *Front Neurosci.* **16**, 852680 (2022).
77. Aimone, J. B. et al. Regulation and Function of Adult Neurogenesis: From Genes to Cognition. *Physiological Rev.* **94**, 991–1026 (2014).
78. Braun, S. M. G. & Jessberger, S. Adult neurogenesis: mechanisms and functional significance. *Development* **141**, 1983–1986 (2014).
79. Amanollahi, M., Jameie, M., Heidari, A. & Rezaei, N. The Dialogue Between Neuroinflammation and Adult Neurogenesis: Mechanisms Involved and Alterations in Neurological Diseases. *Mol. Neurobiol.* **60**, 923–959 (2023).
80. Zhang, W., Xiao, D., Mao, Q. & Xia, H. Role of neuroinflammation in neurodegeneration development. *Sig Transduct. Target Ther.* **8**, 267 (2023).
81. Massagué, J. & Sheppard, D. TGF-β signaling in health and disease. *Cell* **186**, 4007–4037 (2023).
82. Vidovic, N. & Spittau, B. Microglial Transforming Growth Factor-β Signaling in Alzheimer's Disease. *IJMS* **25**, 3090 (2024).
83. Caraci, F. et al. TGF-β1 Pathway as a New Target for Neuroprotection in Alzheimer's Disease: Neuroprotective Role of TGF-β1 in AD. *CNS Neurosci. Therapeutics* **17**, 237–249 (2011).
84. Yin, Z. et al. APOE4 impairs the microglial response in Alzheimer's disease by inducing TGFβ-mediated checkpoints. *Nat. Immunol.* **24**, 1839–1853 (2023).
85. Doyle, K. P., Cekanaviciute, E., Mamer, L. E. & Buckwalter, M. S. TGFβ signaling in the brain increases with aging and signals to astrocytes and innate immune cells in the weeks after stroke. *J. Neuroinflammation* **7**, 62 (2010).
86. Fuster-Matanzo, A., Llorens-Martín, M., Hernández, F. & Avila, J. Role of Neuroinflammation in Adult Neurogenesis and Alzheimer Disease: Therapeutic Approaches. *Mediators Inflamm.* **2013**, 1–9 (2013).
87. Zera, K. A. & Buckwalter, M. S. The Local and Peripheral Immune Responses to Stroke: Implications for Therapeutic Development. *Neurotherapeutics* **17**, 414–435 (2020).

88. Sterner, R. C. & Sterner, R. M. Immune response following traumatic spinal cord injury: Pathophysiology and therapies. *Front. Immunol.* **13**, 1084101 (2023).
89. Kuhn, H. G. Control of Cell Survival in Adult Mammalian Neurogenesis. *Cold Spring Harb Perspect Biol* a018895 (2015) https://doi.org/10.1101/cshperspect.a018895.
90. Culig, L. et al. Increasing adult hippocampal neurogenesis in mice after exposure to unpredictable chronic mild stress may counteract some of the effects of stress. *Neuropharmacology* **126**, 179–189 (2017).
91. O'Kusky, J. R., Ye, P. & D'Ercole, A. J. Insulin-Like Growth Factor-I Promotes Neurogenesis and Synaptogenesis in the Hippocampal Dentate Gyrus during Postnatal Development. *J. Neurosci.* **20**, 8435–8442 (2000).
92. Yu, D. et al. Microglia regulate GABAergic neurogenesis in prenatal human brain through IGF1. *Nature* **646**, 676–686 (2025).
93. Zhang, J. et al. IL4-driven microglia modulate stress resilience through BDNF-dependent neurogenesis. *Sci. Adv.* **7**, eabb9888 (2021).
94. Vivar, C., Potter, M. C. & van Praag, H. All About Running: Synaptic Plasticity, Growth Factors and Adult Hippocampal Neurogenesis. *Curr. Top. Behav. Neurosci.* **15**, 189–210 (2013).
95. Amiri, A. et al. *Pten* Deletion in Adult Hippocampal Neural Stem/Progenitor Cells Causes Cellular Abnormalities and Alters Neurogenesis. *J. Neurosci.* **32**, 5880–5890 (2012).
96. Zeng, L.-H., Rensing, N. R. & Wong, M. The Mammalian Target of Rapamycin Signaling Pathway Mediates Epileptogenesis in a Model of Temporal Lobe Epilepsy. *J. Neurosci.* **29**, 6964–6972 (2009).
97. Buckmaster, P. S. & Lew, F. H. Rapamycin suppresses mossy fiber sprouting but not seizure frequency in a mouse model of temporal lobe epilepsy. *J. Neurosci.* **31**, 2337–2347 (2011).
98. Butler, C. R., Boychuk, J. A. & Smith, B. N. Effects of Rapamycin Treatment on Neurogenesis and Synaptic Reorganization in the Dentate Gyrus after Controlled Cortical Impact Injury in Mice. *Front. Syst. Neurosci.* **9**, (2015).
99. Jin, Y., Barnett, A., Zhang, Y., Yu, X. & Luo, Y. Poststroke Sonic Hedgehog Agonist Treatment Improves Functional Recovery by Enhancing Neurogenesis and Angiogenesis. *Stroke* **48**, 1636–1645 (2017).
100. Andermatt, I. et al. Semaphorin 6B acts as a receptor in post-crossing commissural axon guidance. *Development* **141**, 3709–3720 (2014).
101. Tawarayama, H., Yoshida, Y., Suto, F., Mitchell, K. J. & Fujisawa, H. Roles of semaphorin-6B and plexin-A2 in lamina-restricted projection of hippocampal mossy fibers. *J. Neurosci.* **30**, 7049–7060 (2010).
102. Chang, X. et al. ZMYND11 functions in bimodal regulation of latent genes and brain-like splicing to safeguard corticogenesis. *Nat. Commun.* **16**, 9010 (2025).
103. Garthe, A., Roeder, I. & Kempermann, G. Mice in an enriched environment learn more flexibly because of adult hippocampal neurogenesis. *Hippocampus* **26**, 261–271 (2016).
104. Berdugo-Vega, G., Lee, C.-C., Garthe, A., Kempermann, G. & Calegari, F. Adult-born neurons promote cognitive flexibility by improving memory precision and indexing. *Hippocampus* **31**, 1068–1079 (2021).
105. Madisen, L. et al. A robust and high-throughput Cre reporting and characterization system for the whole mouse brain. *Nat. Neurosci.* **13**, 133–140 (2010).
106. Larsson, J. et al. Abnormal angiogenesis but intact hematopoietic potential in TGF-β type I receptor-deficient mice. *EMBO J.* **20**, 1663–1673 (2001).
107. Levéen, P. et al. Induced disruption of the transforming growth factor beta type II receptor gene in mice causes a lethal inflammatory disorder that is transplantable. *Blood* **100**, 560–568 (2002).
108. Pasparakis, M., Alexopoulou, L., Episkopou, V. & Kollias, G. Immune and inflammatory responses in TNF alpha-deficient mice: a critical requirement for TNF alpha in the formation of primary B cell follicles, follicular dendritic cell networks and germinal centers, and in the maturation of the humoral immune response. *J. Exp. Med.* **184**, 1397–1411 (1996).
109. Liu, J.-L. et al. Insulin-Like Growth Factor-I Affects Perinatal Lethality and Postnatal Development in a Gene Dosage-Dependent Manner: Manipulation Using the Cre/loxP System in Transgenic Mice. *Mol. Endocrinol.* **12**, 1452–1462 (1998).
110. Srinivas, S. et al. Cre reporter strains produced by targeted insertion of EYFP and ECFP into the ROSA26 locus. *BMC Dev. Biol.* **1**, 4 (2001).
111. Bedolla, A. et al. Diphtheria toxin induced but not CSF1R inhibitor mediated microglia ablation model leads to the loss of CSF/ventricular spaces in vivo that is independent of cytokine upregulation. *J. Neuroinflammation* **19**, 3 (2022).
112. Joseph, E. *et al*. Design, Synthesis and Preclinical Evaluation of a Brain-Permeable PET Tracer for P2Y12 Receptor Imaging in the Brain. *J Med Chem* **68**, 15543–15562.
113. Taranov, A. et al. The choroid plexus maintains adult brain ventricles and subventricular zone neuroblast pool, which facilitates poststroke neurogenesis. *Proc. Natl. Acad. Sci. Usa.* **121**, e2400213121 (2024).
114. Romagnolo, A. et al. Astroglial calcium signaling and homeostasis in tuberous sclerosis complex. *Acta Neuropathol.* **147**, 48 (2024).
115. Korsunsky, I. et al. Fast, sensitive and accurate integration of single-cell data with Harmony. *Nat. Methods* **16**, 1289–1296 (2019).
116. Ware, K., Peter, J., McClain, L. & Luo, Y. Cell type–dependent role of transforming growth factor-β signaling on postnatal neural stem cell proliferation and migration. *Neural Regen. Res* **21**, 1151–1161 (2025).
117. Luo, F. et al. Cuprizone-induced demyelination under physiological and post-stroke condition leads to decreased neurogenesis response in adult mouse brain. *Exp. Neurol.* **326**, 113168 (2020).

Acknowledgements

We thank Chet Closson and the University of Cincinnati live imaging core (supported by NIH S10OD030402) for technical support. We thank Lucas McClain, who maintained and genotyped mouse colonies used in this study. Y.L is supported by NIH grants (R01NS125074 and R01AG083164). K.W. was supported by NIH 1F31NS129204-01A1. J.P. is supported by the Dean's Dissertation Completion Fellowship (no specific grant number).

Author contributions

Y.L. and K.W. conceptualized the study and designed the experiments. K.W. performed tamoxifen administration or rapamycin treatment on the *Cx3cr1CreER-Alk5* and *P2ry12CreER-Alk5*, the *Tnf* double KO and the *Igf1* double KO and control mice, recorded and analyzed data for the immunohistochemistry, FACS sorting of microglia and tissue collection for scRNAseq. J.P. performed tamoxifen injection, qRT-PCR quantification of sorted microglia, blood, and splenic monocytes, IHC quantification of oligodendrocytes, the in vitro NSC and primary microglia 3D co-culture, and some behavioral tests. J.Y. performed some behavioral tests in microglial-receptor iKO mice and analysis of microglia count in the PLX experiment. A.T. performed unbiased immunohistochemistry analysis of microglia and astrocytes and proliferating microglia. A.B. and C.D performed some behavioral tests in microglial-ligand and receptor KO mice. Sven L, R.F and A.S generated and validated the P2RY12 antibodies, K.R., C.T. S.L and K.W. analyzed the scRNAseq data and data presentation. K.W. and Y.L drafted and J.P, Y.L and S.L revised and edited

the paper. All authors read, edited, and approved the final version of the manuscript.

Competing interests
The authors declare no competing interests.

Additional information
Supplementary information The online version contains supplementary material available at https://doi.org/10.1038/s41467-026-68885-4.

Correspondence and requests for materials should be addressed to Yu Luo.

Peer review information *Nature Communications* thanks Björn Spittau and the other, anonymous, reviewers for their contribution to the peer review of this work. A peer review file is available.